博士論文

Functional differentiation in the monkey brain network for memory encoding and retrieval revealed by functional magnetic resonance imaging

（磁気共鳴機能画像法によるマカクザルの大脳皮質記憶回路における機能分化の解明）

宮本　健太郎

Functional differentiation in the monkey brain network for memory encoding and retrieval revealed by functional magnetic resonance imaging

磁気共鳴機能画像法によるマカクザルの大脳皮質記憶回路における機能分化の解明

所属：　医学系研究科　機能生物学専攻　統合生理学

指導教員：　宮下　保司　教授

申請者：　宮本　健太郎

Index

Abstract

Functional magnetic resonance imaging (fMRI) previously revealed the involvement of various cortical regions including the posterior parietal cortex (PPC) and medial temporal lobe (MTL) in human memory processing: retrieval and encoding. However, the corresponding memory-related networks have not been identified in monkeys. In this thesis, awake monkey fMRI, which captures whole-brain activity using an identical paradigm to human studies, was utilized to identify the networks. To localize the memory retrieval network, cortical activity comparisons were made during the correct recognition of previously seen items and rejection of unseen items. Two major PPC activation sites were uncovered that contribute to the retrieval of differentially-positioned items on a list of sequentially presented pictures: area PG/PGOp in inferior parietal lobule (IPL), along with the hippocampus, was more active for initial item retrieval, while area PEa/DIP in intraparietal sulcus (IPS) was for the last item. Moreover, connectivity from the hippocampus to the PG/PGOp, but not the PEa/DIP, increased during initial item retrieval. Furthermore, the two parietal areas participated in different memory sub-networks, extracted based on functional connectivity among brain-wide retrieval-related regions. To localize the memory encoding network, memory traces predictive of subsequent memory retrieval performance were identified within the caudal entorhinal cortex (cERC) and perirhinal cortex (PRC), both MTL subregions, as well as the hippocampus. Additionally, neuronal activity in the directly-connected cERC/hippocampus, but not the PRC, was responsible for encoding the initial items. These brain region-dependent distinctions involved in memory encoding and retrieval imply a functional correspondence between macaque and human memory networks.

Introduction

Functional magnetic resonance imaging (fMRI) is a non-invasive neuroimaging technique that measures brain activity by detecting changes in cerebral blood flow coupled with neuronal activation. Recent advancement of this non-invasive neuroimaging technique based on BOLD (Blood Oxygenation Level Dependent) signal change that is due to the hemodynamic and metabolic sequelae of neuronal responses has successfully enabled the capture of whole-brain activity in humans, allowing previously unattainable functional measurements related to specific cognitive events (e.g., memory encoding and retrieval), simultaneously with millimeter spatial and one-second time resolution.

On the other hand, the macaque monkey has for decades provided an important model for understanding higher cognitive brain functions, and a wealth of information is now available in terms of fundamental electrophysiology data obtained with microelectrodes, histology mapping of architectonic cortical and subcortical area subdivisions, neural tract tracer pathway reconstructions, and lesions studies. However, the functional localization of memory-related neural activity at a whole-brain level remains unknown in monkeys. Therefore, we cannot directly apply most of the knowledge gleaned from the monkey studies to the interpretation of human fMRI results.

To bridge the gap between the monkey and human data, fMRI of awake monkeys ("awake-monkey fMRI") is beneficial. Awake-monkey fMRI captures whole-brain activity related to specific cognitive processes by using a paradigm identical to that utilized in the human fMRI investigations [1-6]. In the present thesis project, awake-monkey fMRI experiments were conducted, in which macaque monkeys performed memory encoding and retrieval tasks similar to those previously conducted with human subjects. Then, the results were compared between the two species.

Human fMRI studies reported the involvement of various brain regions including the posterior parietal cortex (PPC), the medial temporal lobe (MTL), and the prefrontal cortex (PFC) in memory retrieval [7, 8]. Multiple areas within the PPC show retrieval-related activation when human subjects correctly recognize previously seen items, as compared with correctly identifying unseen new items ("old/new effect") [9, 10]. This old/new effect, which is derived from comparisons of brain activity during the same retrieval period of successful trials, reflects cognitive processes related solely to the retrieval of recognition memory, or the ability to recognize previously encountered events and objects. fMRI studies have dissociated these PPC areas by differences in their cognitive function, as well as by differences in their functional/anatomical connectivity with MTL and PFC. However, unlike MTL and PFC, in which neuropsychological neuropsychological evidence for memory function is abundant (for reviews see Squire et al. [8]), neuropsychological studies have only recently shown that damage to PPC causes mild impairment in episodic retrieval. Neuropsychological clues that dissociate the retrieval processes in PPC remain insufficient due to the limited number of available cases with damage in specific PPC subregions. Therefore I especially focused on the functions of PPC in the present thesis.

Human imaging studies also reported that fMRI signals recorded from the MTL during the encoding of subsequently recognized stimuli ("later Hit items") significantly differed from those recorded during the encoding of subsequently forgotten stimuli ("later Miss items"). This phenomenon is termed the "subsequent memory effect". The cortical regions showing the subsequent memory effect are critical for memory encoding, because trial-by-trial fluctuation of neuronal activity during memory encoding in these regions can substantively predict subsequent recognition performance.

This subsequent memory effect has been repeatedly reported to be localized in the hippocampus and in the perirhinal and parahippocampal cortices within the “parahippocampal region”. However, it remains difficult to precisely localize the loci that underlie the subsequent memory effect within the human parahippocampal region because information on the cytoarchitecture and axonal projections in these cortices is limited in humans, and MRI-based boundary delineation within these regions has not yet been established. Studies of nonhuman primate models are beneficial to address this difficulty, as a wealth of information is available on the electrophysiology, histology, and lesion studies. Especially, the anatomical reference frame in the parahippocampal region is established in the macaque monkeys, which would be helpful for fine localization of memory traces. Therefore I attempted to localize the distribution of memory traces within the macaque parahippocampal region in the present thesis.

In the present fMRI study, I first identified a) the retrieval-related cortical regions of the macaque monkey brain that demonstrates the old/new effect, and b) the encoding-related cortical regions, or memory traces, that predict subsequent recognition performance. I then characterized and compared the response profiles of the identified retrieval- and encoding-related regions of the macaque brain based on the serial position effect, or the “primacy and recency effect”. Monkeys performed the serial probe recognition task in the MRI scanner. During the task, the monkeys were required to view a list of serially presented pictures and to judge whether the test item was seen in any item position on the list (old/new judgment). Behaviorally, memory accuracy in both monkeys and humans show primacy and recency effects that are accompanied by typical U-shaped serial position curves. That is, the accuracy of the retrieval of the first item observed (i.e., the primacy effect) and the accuracy of the retrieval of the last item observed (i.e., the recency effect) are higher than the accuracy of retrieval of any of the other items observed

[11].

Recent human fMRI studies showed that activity in the hippocampus reflects the primacy effect [12, 13]. The existence of serial position effects allowed us to similarly characterize the retrieval-related areas in the macaque PPC, as well as the encoding-related areas in the macaque MTL. In the current thesis investigation, the two retrieval-related parietal areas, one located in the inferior parietal lobule (IPL) and the other located in the intraparietal sulcus (IPS), demonstrated mutually contrasting profiles depending on item position, both in activation and task-evoked connectivity. Encoding-related regions in the MTL also involved two qualitatively distinct processes that critically contributed to encoding items in different positions on a list. These functional distinctions within the macaque PPC and MTL suggested the functional correspondence of the retrieval- and encoding-related networks between monkeys and humans.

Part I

Retrieval-related network in macaque monkeys

Materials and Methods

Subjects

Two monkeys (*Macaca fuscata*; Monkey A: female, 6 kg; Monkey V: male, 8 kg) participated in the experiment. Before fMRI scanning, an MRI-compatible version of a ring-type head fixation device [14] was attached to the monkeys. This fixation device consisted of an acrylic head ring mounted with six screw holders. It was firmly fixed to the animal's skull with six plastic screw pins (RENY). This dental cement free device was robust to signal loss of MR images caused by magnetic field inhomogeneity. Surgery for attachment of the head-fixation device was conducted in aseptic conditions under general anesthesia with sodium pentobarbital (5 mg/kg/h, i.v.) and xylazine (2 mg/kg, i.m.), supplemented as needed. Monkeys were given postsurgical analgesics (ketoprofen, 1 mg/kg/day, i.m.) for at least three days, and postsurgical prophylactic antibiotics (benzylpenicillin, 20,000 unit/kg/day, ampicillin, 100 mg/kg/day, i.m. or enrofloxacin, 5mg/kg/day, subcutaneous injection) for one week as described previously [15, 16]. All the experimental protocols were in full compliance with the regulations of the University of Tokyo School of Medicine and with the NIH guidelines for the care and use of laboratory animals.

Experimental setup for behavioral testing

The monkeys performed a serial probe recognition task [11] modified for fMRI (see Figure 1A). Initially they were trained and adapted to perform the task in a mock scanner and inside the magnet bore as described previously [2, 4]. fMRI experiments were started when the monkey was consistently able to distinguish “seen” and “unseen” items in the retrieval task in the MRI scanner.

Online behavioral control and reward delivery were implemented in the Presentation platform

(Neurobehavioral Systems, CA) as described previously [17]. For the stimuli, 1,000 pictures of natural or artificial objects selected from the HAMERA Photo-Object database (Source Next, Tokyo) were used, which were cropped and presented to the animals at 3.6 × 3.6 degrees in visual angle. Typically, each picture was presented in only one trial (two trials at most) in each session. Pilot experiments confirmed that the second presentation did not affect task performance. In a custom-made MRI-compatible monkey chair (Nakazawa, Tokyo), the monkey manipulated an optic fiber-based, custom-made three-way joystick with one of its forelimbs. An optic fiber-based photoelectric sensor (Omron, Tokyo) was used to monitor the movements of each of the other three limbs. Eye position was monitored at 120 Hz with an infrared-sensitive CCD camera (ISCAN, MA).

Behavioral tasks

The monkeys performed a serial probe recognition task [11] modified for fMRI (see Figure 1A). Each trial began with the presentation of a fixation point after the monkey pulled the joystick ("Warning", see Figure 1A). The list items then appeared serially ("Cue 1–4"). Each item was presented at the center of the monitor for 1 s followed by interstimulus intervals of 1 s. The items were selected from the 1,000-picture pool in a pseudo-random order. Typically, each picture was presented in only one trial (two trials at most) in each session. The last list item was followed by a delay period variably changed trial-by-trial between 7 and 10 s ("Delay"). Finally, the monkey was presented with one test item at the center and two symbols, a triangle and a cross, on the left and right sides of the image ("Choice"). The assignment of symbols to the left or right side was randomly selected trial by trial. In half the trials, the item in the choice period was the same as one of the cue items, and in the other half of trials, the item had not been presented as a cue item.

Monkeys responded by moving the joystick in the "seen" symbol direction (a triangle for monkey A and a cross for monkey V) if the test item was from the cue item list, or by moving the joystick in the "unseen" symbol direction (a cross for monkey A and a triangle for monkey V) if it was not from the list. The monkey received juice drops, accompanied by a distinctive secondary visual reinforcement ("Feedback"). Incorrect choices resulted in termination of the trial without reward. Trials were separated by a 4-s intertrial interval, during which the screen was black. If any limbs moved during the trials, the optic sensors detected the movement and the trial was aborted immediately. At the first stage of experiments, which lasted for 24–26 sessions, the monkeys performed a single-probe recognition task (number of cue items = 1) to localize retrieval-related regions (see Figure 2A). The task procedure was the same as above but used a single item for the cue. The monkeys then performed the serial probe recognition task (number of cue items = 4).

Data acquisition

Functional images were acquired in a 4.7-T MRI scanner (Biospec 47/40, Bruker, Ettlingen) with 100 mT/m actively shielded gradient coils and a transceiver saddle RF coil (Takashima, Tokyo) [16, 18-20]. In each session, functional data were acquired using a gradient-echo echo-planar imaging (EPI) sequence (1-shot, TR = 2.5 s, TE = 20 ms, 1.25×1.5 mm^2 in-plane resolution, 64×96 matrix, slice thickness = 1.5 mm with inter-slice gap = 0.25 mm, 27 horizontal slices covering the whole brain). The activation peak identified in a part of the lateral temporal cortex was not included in the following analyses, because these areas partially suffered from signal decrease due to magnetic field inhomogeneity. T2-weighted spin-echo (RARE) images with the same geometry as the EPI were also scanned.

In the experiments using the serial probe recognition task, each run consisted of 237 functional volumes (10 min; the first three volumes were discarded), including 20–25 trials. In the experiments using the single-probe recognition task, each run consisted of 141 volumes (6 min; the first three volumes were discarded), including 15–20 trials.

To assess spontaneous functional connectivity between the retrieval-related regions detected in the above fMRI sessions, fMRI data under anesthesia were collected from the same monkeys used for the recognition memory experiments [18, 19, 21]. We determined the localizations of the retrieval-related areas and evaluated their connectivities in the same monkeys. Anesthesia was introduced with an intramuscular injection of medetomidine/midazolam (30 μg/kg and 0.3 mg/kg, respectively) and maintained with continuous intravenous infusion of propofol (6–10 mg/kg/h) before the MRI experiments. During the acquisition of functional images, anesthesia was switched to and maintained with continuous intravenous infusion of dexmedetomidine (10–15 μg/kg/h). Heart rate, oxygen saturation, respiration rate/EtCO2, and blood pressure were continuously monitored. Body temperature was kept constant using a bag with circulating hot water. Lactated Ringer's solution containing 5% glucose was given intravenously (5 mL/kg/h) throughout the experiment. Each session consisted of 14 runs of 357 functional volumes (15 min; the first three volumes discarded). In each monkey, two sessions were performed, and a total of 9,996 volumes were analyzed.

Resting-state data in awake condition was also collected from the same monkeys used for the recognition memory experiments. During the acquisition of functional images, the movements of each of the four limbs were monitored. The monkeys were rewarded as long as all limbs stay motionless at intervals of 3–5s.

In separate sessions, high-resolution T1-weighted structural images of the monkeys were

scanned using the 3D-MDEFT sequence (0.5 mm isotropic). High-resolution EPI (32-shot, TR = 3 s, TE = 20 ms, 0.625 × 0.75 mm^2 in-plane resolution, 128 × 192 matrix, slice thickness = 0.75 mm with inter-slice gap = 0.13 mm, 54 horizontal slices covering the whole brain) was also acquired to serve as the template image for spatial normalization (see below).

Identification of retrieval-related regions

The retrieval-related regions were identified by performing voxel-wise GLM analyses implemented in SPM5. These analyses included the following predictors: the choice onsets for (1) Hit trials (correctly recognized seen items), (2) CR trials (correctly rejected unseen item), (3) Miss trials (seen items endorsed as unseen), and (4) FA trials (unseen items endorsed as seen); (5–9) the cue onsets in Hit, CR, Miss, FA, and other (aborted) trials; and (10) the timing of other types of errors (including body movements detected by the optic sensors and responses before the choice period). These events were modeled as delta functions convolved with the canonical hemodynamic response function and its temporal and dispersion derivatives. The six parameters of head motion derived from realignment were also included in the model as covariates of no interest. Data were high-pass filtered using a cutoff of 32 s. Data from 24 sessions for Monkey A and 26 sessions for Monkey V were analyzed. The group analysis of the data from the two monkeys was conducted by using a fixed-effect model. Retrieval-related regions were identified as the group analysis map (see Figure 3A) of the comparison of BOLD signals between the Hit and CR conditions [9]. Activation peaks listed in Table 2 were detected in the following steps (see also [22]). The group analysis map was smoothed using a 3-mm kernel, and then the location of peaks exceeding $p < 0.001$ significance were searched. Peaks separated by less than 4 mm were concatenated by averaging coordinates. The coordinates of the activation peaks at

which the t value in the group analysis map was significant at $p < 0.01$ with FDR correction are included in Table 2 [23]. These peaks were labeled by referring to the atlas of Paxinos et al. [24] (see Table 1). The region of interest (ROI) for each peak was defined as the significant voxels within a 2-mm radius ($p < 0.01$ with FDR correction).

To determine the precise locations of the activation peaks in the IPS, voxel-wise GLM analysis was conducted by using functional images without spatial smoothing. This analysis was performed separately in each monkey by using individual EPI images as templates for spatial normalization. The locations of activation peaks were confirmed in both the axial (see Figure 4A) and coronal (see Figure 4B) planes of the individual EPI images.

To examine the reproducibility of the results from two monkeys, a conjunction map (conjunction null, $p < 0.05$, FDR corrected) of retrieval-related regions was generated. The conjunction showed commonly activated areas that satisfied $p < 0.05$ (FDR corrected) for each monkey [25, 26].

Nomenclatures of retrieval-related areas in PPC

For the two PPC areas, PG/PGOp and PEa/DIP, we confirmed the locations of peaks with coordinate registrations in Caret software (version 5.61; http://brainvis.wustl.edu/wiki/index.php/Caret:About) [27, 28]. The bilateral peaks of the activation site in the IPL corresponded to ‘PG’, while the bilateral peaks in the IPS corresponded to ‘PEa’ according to the classifications made by [29], as well as [24]. However, ‘PG’ and ‘PEa’ are defined as a wide area in these classifications. The retrieval-related activity was detected in subregions of these wider areas. In the IPL, the activation site spread on ventral part of PG adjacent to lateral sulcus and that straddled the border with PGOp. In IPS, the activation site was

in the ventral part of the medial bank of the intraparietal sulcus and that straddled the border with DIP. Therefore to describe the specific localization of retrieval-related activities properly, we termed these areas ‘PG/PGOp’ and ‘PEa/DIP’, respectively.

Analysis of experiments using the serial probe recognition task

Functional images acquired in experiments using the serial probe recognition task were preprocessed like those of the single-probe recognition task. In this serial probe recognition task, Hit and Miss trials were further classified respectively into four categories according to the item position in the cue sequence in which the tested image in the choice period was presented (Hit1–Hit4 and Miss1–Miss4). In a Hit [Miss] trial, the item in the cue sequence that matched the test item was defined as a subsequent Hit [subsequent Miss] cue item. Thus, voxel-wise GLM analyses included the following events: choice onsets for (1–4) Hit1–Hit4 trials, (5) CR trials, (6–9) Miss1–Miss4 trials, and (10) FA trials; the onsets of (11–14) subsequent Hit cue 1–4, (15–18) subsequent Miss cue 1–4, and (19–22) other cue 1–4; and (23) other types of errors. Data from 15 sessions for Monkey A and 11 sessions for Monkey V were analyzed. The retrieval activities in the serial recognition task were measured in each ROI defined in Table 2 using the MarsBaR ROI toolbox for SPM (http://marsbar.sourceforge.net/). Importantly, differential retrieval activity for cue items in different position was evaluated by using ROIs defined in the independent experiment (single-probe recognition task).

Evaluations of primacy- and recency- effect related activity

To examine the effect of cue item position on the retrieval-related activities in each homotopic pair of ROIs in the hippocampus and posterior parietal cortex (left mHC and right pHC; bilateral

PG/PGOp; bilateral PEa/DIP), an across-session repeated-measures MANOVA (four levels of retrieved cue item positions × two hemispheres × two monkeys) of the percentage of BOLD signal changes at each of the choice onsets of Hit1–Hit4 trials was conducted using SPSS Statistics 20.0 (IBM, NY), which included the factors of retrieved cue item position (Hit1, 2, 3, 4), hemisphere (left, right), and monkey (Monkey A, Monkey V). For the regions with significant main effect only for cue item position (not for hemisphere or monkey), to assess the activity enhancement in the retrieval of the initial and last items in the cue sequence (primacy effect-related and recency effect-related activity, respectively) across sessions, the following regression analyses were performed for each ROI:

$$y_i = \alpha_{pi} + \beta_{pi} n_p + \varepsilon_{pi} \qquad \text{(Equation 1)}$$

$$y_i = \alpha_{ri} + \beta_{ri} n_r + \varepsilon_{ri} \qquad \text{(Equation 2)}$$

where in a session *i*, each component of a 4-component vector, y_i, represents the signal change in the retrieval of cue items in each position (Hit1, 2, 3, 4); n_p is the "primacy predictor", defined by [1, 0, 0, 0] and n_r is the "recency predictor", defined by [0, 0, 0, 1]; α_{pi} and α_{ri} are constants; ε_{pi} and ε_{pi} are error terms; and β_{pi} and β_{ri} are the estimated values for the "serial position effect"-related activity for n_p and n_r, respectively. For each homotopic pair of ROIs, β_p [β_r] was calculated as the mean of β_{pi} [β_{ri}] across sessions, hemispheres, and monkeys. The homotopic ROI pairs with $\beta_p > 0$ were defined as primacy effect-related, and pairs with $\beta_r > 0$ were defined as recency effect-related. The criterion for the statistical significance of β_p and β_r was $p < 0.05$ with Bonferroni correction for two independent tests.

For PG/PGOp and PEa/DIP, which shows a U-shaped curve of retrieval-related activity for each cue item in a list, the following multiple regression analyses using both of the predictors were also performed:

$$y_i = \alpha_{upi} + \beta_{upi} n_p + \varepsilon_{upi} \qquad \text{(Equation 3)}$$

$$y_i = \alpha_{uri} + \beta_{uri} n_r + \varepsilon_{uri} \qquad \text{(Equation 4)}$$

where α_{upi} and α_{uri} are constants; ε_{upi} and ε_{upi} are error terms; and β_{upi} and β_{uri} are the estimated values for the "serial position effect"-related activity with a U-shaped response profile curve for n_p and n_r, respectively.

Psychophysiological interaction (PPI) analysis

To examine the effect of item positions in the cue sequence on effective connectivity between the hippocampus and the two posterior parietal retrieval-related regions (PG/PGOp, PEa/DIP), PPI analyses[30] were conducted for the serial probe recognition task using SPM5. The "physiological" time series extracted at the hippocampus was corrected for variance associated with parameters of no interest, deconvolved with the hemodynamic responses, multiplied by a parameter encoding the relevant "psychological" contrast (Hit1 > Hit4), and reconvolved to form a "psychophysiological interaction" ("PPI") predictor. These three predictors ("physiological" time series, "psychological" contrast, and "PPI") were entered into a design matrix alongside parameters encoding the main effects of the other choice onset and cue onset predictors, as well as the same nuisance predictors used for the voxel-based GLM analysis of the serial probe recognition experiments. The effect size of the PPI at the two parietal regions with the seed at the hippocampus was evaluated as the beta estimate for the "PPI" predictor averaged across all sessions from the two monkeys, and the statistical threshold was set at $p < 0.05$ (FWE corrected within each region).

Similarly, another PPI analysis was conducted to examine the effect of item positions in the cue sequence on effective connectivity from the two posterior parietal retrieval-related regions

(PG/PGOp, PEa/DIP) to V4 in the contrast Hit4 > Hit2 (see Figure 6). The effect size of the PPI was evaluated as similarly described above. Area 9/46V, which is one of the retrieval-related areas identified in this study, is known as a center of top-down attention in macaque prefrontal cortex [31]. Monkey area V4 is anatomically connected to area 9/46V via FEF[32]. Therefore the target area within V4 was identified by the PPI analysis (Hit4 > Hit2) with the seed on the retrieval-related area of right 9/46V (Hit > CR; listed in Table 2) (see Figure 6A). We defined the target ROI in V4 as the significant voxels that shows retrieval-related activity (Hit > CR; FDR-corrected $p < 0.05$) within a 2-mm radius from the peak identified in V4 by the PPI analysis from area 9/46V.

Functional connectivity analysis of BOLD activity

In addition to standard preprocessing steps as described above for task-based MRI, functional images of spontaneous activity under anesthesia underwent several additional preprocessing steps for intrinsic correlation analyses, as described previously[16, 18, 19]. The time series from each BOLD run were temporally filtered to retain frequencies in the $0.0025 < f < 0.05$ Hz band [21]. Several sources of spurious variance were removed from the filtered time series by regression of nuisance variables including six parameters obtained by realignment and the signals averaged over the whole brain and ventricles[21, 33, 34]. Then the BOLD time series for each of the retrieval-related ROIs was calculated by averaging time series over all voxels in each of the ROIs. A Pearson correlation coefficient matrix between all ROIs was then calculated across the two monkeys and defined as functional connectivity among them (see Figure 7B).

Functional connectivity analysis of resting state in the awake condition

We assessed functional connectivity of resting state in the awake condition from two additional types of datasets (see Figure 8B) in the same two monkeys used for the recognition tasks. The first dataset (see Figure 8B, middle row) was collected in the experiments where the monkeys were imposed to stay still in the scanner (see *Data acquisition*). The second (see Figure 8B, lower row) was the residual time courses from the serial probe recognition task dataset (remaining signal after task events were regressed out). It has been shown that the correlation of the remaining signals is similar to that of resting state data [35, 36]. For each of these two datasets, after the same preprocessing as the anesthetized condition and artifact reduction with spatial independent component analysis [37, 38] (GIFT software, http://mialab.mrn.org/software/gift/index.html), Pearson correlation maps at the voxel level were generated for the seed ROIs of PG/PGOp (see Figure 8B, red) and PEa/DIP (see Figure 8B, blue) as described above.

Anatomical connections of PPC areas

The spatial distributions of anatomical connections of IPL and medial IPS in Figure 7A were mapped based on tracer injection data of Lewis and Van Essen [39], which includes injection sites (Case D in IPL and Case A in medial IPS) that are cytoarchitectonically close to the two retrieval-related areas (PG/PGOp in IPL and PEa/DIP in medial IPS) in the present study. The projection density data, which were distributed with Caret software and a monkey brain atlas (F99), were nonlinearly registered onto our Monkey A's template image by using SPM5.

With the aid of CoCoMac database (collection of past tracer studies in the macaque cerebral cortex) [40], we further examined whether PG/PGOp and PEa/DIP have axonal connections with each of all the cortical areas labeled in Paxinos et al. [24]. The results are presented in Figure 8A,

where we excluded cortical areas for which CoCoMac has no data about the presence or absence of connections with both of PEa/DIP and PG/PGOp. Because of a relative lack of data about interhemispheric connections in CoCoMac, only intrahemispheric axonal projections are shown in Figure 8A, and functional connectivity is correspondingly shown only for intrahemispheric connections in Figure 8A.

Module Optimization analysis

Graph theory-based analyses on the functional connectivity matrix were performed to test whether distinct groups or "modules" existed within the network of functional connectivity among the retrieval-related regions, which might provide further distinctions between the ROIs of the retrieval-related regions. Each ROI corresponded to an element, or "node", in the network, and the connection between each pair of ROIs corresponded to a link, or "edge". Module detection was performed with an algorithm that optimizes "modularity" [41, 42]. This algorithm divided retrieval-related regions into non-overlapping groups of ROIs to maximize the total weight of within-group edges compared to that expected by chance (modularity metrics [Q]) and minimize the total weight of between-group edges, by considering both the positive and negative weight of connectivity without any thresholding. The algorithm maximizes the Q metric and returns the node assignments into modules that yield the highest value. The data were calculated with SPM5 and the Brain Connectivity Toolbox [43] on MATLAB. For display purposes, the module assignments were presented on an inflated representation of monkey A's anatomical template, using Caret software (see Figure 7D).

Evaluations of primacy- and recency- effect related activity for each module

For each of the detected modules of the retrieval-related areas, whether modulation of the gross retrieval activity within the module depended on the item positions in the cue sequence was examined by conducting a repeated-measures MANOVA for the signal changes at the choice onsets of Hit1–Hit4 trials from all the ROIs comprising the module. The statistical design included the factors of retrieved cue item position (Hit1, 2, 3, 4), monkey (Monkey A, Monkey V), and ROI (each ROI included in the module), and the main effect of the retrieved cue item position was tested. For this analysis, the percent signal changes (PSC) of each ROI were normalized to eliminate the variability of the signal across sessions from two monkeys using the following equation: normalized PSC = (raw PSC – min. PSC) / (max. PSC – min. PSC), where max. [min.] is the maximum [minimum] of all the PSCs of an ROI from the same session. For modules that showed a significant main effect of retrieved cue item position without significant interaction with monkey or ROI in the MANOVA, regression analyses were also conducted to identify the neural correlates of primacy and recency effects by using Equation 1 and 2. For modules 2 and 3, which shows U-shaped response profile, multiple regression analyses were conducted additionally by using Equation 3 and 4. For each module, β_p [β_r] was calculated as the mean of β_{pi} [β_{ri}] across sessions, ROIs, and monkeys. The criterion for the statistical significance of β_p and β_r was $p < 0.05$ with Bonferroni correction for two independent tests.

Results

Behavioral results

We conducted fMRI in two macaque monkeys performing a serial probe recognition task with a list of four items (Figure 1A) and a single-probe recognition task (Figure 2A). In these tasks, monkeys were required to judge whether or not the item in the choice period was seen on the list of items presented during the cue period. In the single-probe recognition task, "corrected recognition rate" (defined as "Hit rate" – "False Alarm [FA] rate") (Wagner et al., 1998) was significantly positive (chi-square test; $p < 0.001$ for both monkeys) (Figure 2B, upper panels), suggesting that the monkeys adequately distinguished seen items from unseen items based on items retrieved from memory. Hit rate and Correct Rejection (CR) rate were not significantly different (chi-square test; Monkey A: $p = 0.63$, Monkey V: $p = 0.31$). Reaction times for Hit and CR responses were not significantly different (paired t test (across sessions); Monkey A: $t(23) = -1.44$, $p = 0.16$; Monkey V: $t(25) = 1.26$, $p = 0.21$) (Figure 2B, lower panels). In the serial probe recognition task, the corrected recognition rate for each position of the cue item (Hit1 to Hit4) was significantly positive for both monkeys (chi-square test; $p < 0.05$, for each item of both monkeys) (Figure 1B, upper panels). In addition, the Hit rate was significantly different across the four item positions of the cue (chi-square test; Monkey A: $\chi^2(3) = 9.05$, $p = 0.02$, Monkey V: $\chi^2(3) = 9.98$, $p = 0.01$). Consistent with previous behavioral studies in humans and monkeys, U-shaped serial position curves of the percentage of correct responses were obtained in both monkeys, indicating the presence of "primacy" and "recency" effects in the recognition task[11, 44]. To test the statistical significance of primacy and recency effects in the U-shaped serial position curve, the accuracy on the first list position (Hit1), the last list position (Hit4) and the least accurate of the two middle positions (Hit2 or Hit3) were compared for each monkey[44].

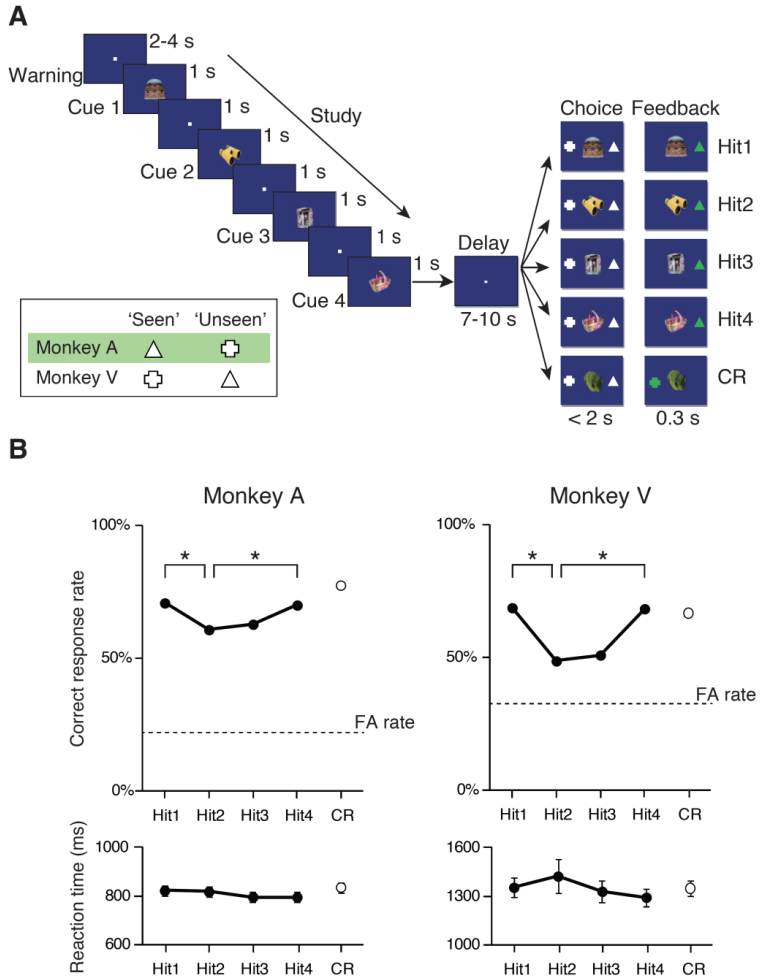

Figure 1. Serial Probe Recognition Task and Behavioral Performance of Monkeys

(A) Trial structure in the serial probe recognition task. In each trial, monkeys pulled the joystick to initiate the trial (Warning), and then four objects to study were sequentially presented (Cue1–4). After a 7–10-s delay (Delay), two choice symbols were presented with a test object (Choice). The symbols, a triangle and a cross, were defined as "seen" and "unseen" symbols for each monkey (see 'inset table'). Monkeys were required to select the "seen" [or "unseen"] symbol if the test object was [was not] included in the studied list of objects. The classification of Hit and CR trials in the case of the symbol definition in Monkey A is shown here.

(B) Serial position curves of behavioral performance for each monkey during scanning sessions. Upper panels show serial position curves for the percentage of correct responses. Each dot represents the Hit rate (●) or CR rate (○). In both monkeys, the Hit rate showed a U-shaped curve as a function of the item position (i.e., the position in the object list) in which the tested item (i.e., test object) was presented in the studied list. Hit rates for each item position significantly exceeded the FA rate (dashed line) (all $p < 0.05$). Lower panels show reaction times (●, Hit trials; ○, CR trials). *: $p < 0.05$ (chi-square test, Ryan's correction). Error bars: SEM across sessions.

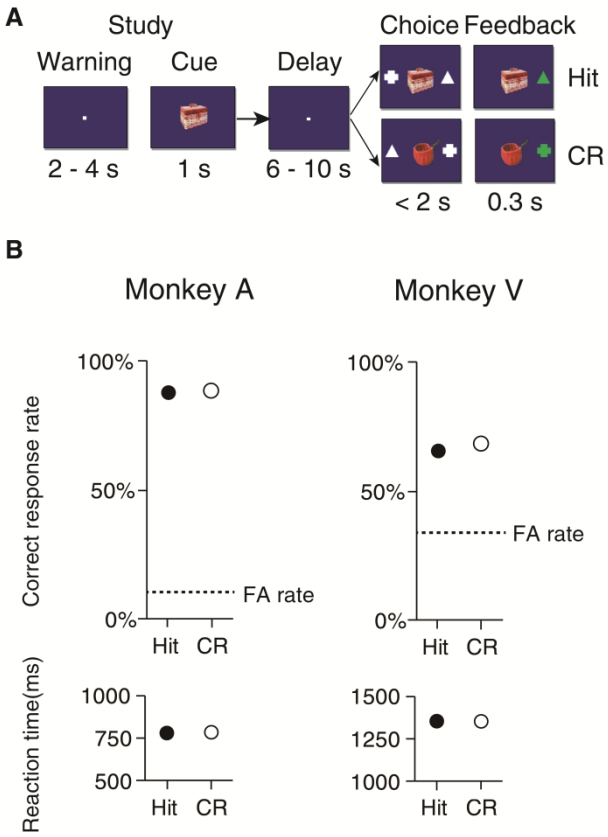

Figure 2. Tasks and behavioral results for the single-probe recognition task

(A) Trial structure of the single-probe recognition task. The classification of Hit and CR trials in the case of the symbol definition in Monkey A is shown here.

(B) Behavior results of each monkey. In the upper panels, each dot represents the Hit rate (●) or CR rate (○). Hit rate significantly exceeded the FA rate (dashed line) ($p < 0.05$ for all). In the lower panels, each dot represents reaction time. Error bars: SEM across sessions (some are smaller than the size of dots).

For both monkeys, the Hit1 and Hit4 rates were significantly higher than the Hit2 rate, which was the least accurate (chi-square test; $p < 0.05$, Ryan's correction). Additionally, no significant difference between the Hit1 and Hit4 rates was observed in either monkey (chi-square test; $p > 0.5$, Ryan's correction). No significant main effect of the position on reaction time was observed (one-way repeated ANOVA (across sessions); Monkey A: $F(3,45) = 2.27$, $p = 0.09$, Monkey V: $F(3,30) = 0.58$, $p = 0.63$) (Figure 1B, lower panels).

Identification of retrieval-related regions

The cortical regions activated by correct recognition of previously presented items (Hit) compared to correct identification of previously unseen items (CR) in the single-probe recognition task in monkeys is shown in Figure 3A (Hit vs. CR). In total, 47 significant activation peaks were detected (Tables 1, 2, $p < 0.01$, fixed effect, corrected for false discovery rate [FDR]). In the PPC, the strongest activation was found bilaterally in the IPS (PEa/DIP, see also "Nomenclatures of retrieval-related areas in PPC" in **Materials and Methods** in **Part I**). In both monkeys, these bilateral peaks in the posterior IPS were located on the medial bank, which is more clearly confirmed in the activation maps generated from unsmoothed functional images (Figure 4). The posterior IPL (PG/PGOp) was also activated bilaterally. In the frontal cortex, the anterior bank (area 45B) and posterior bank (area 6VR [ventral premotor, F5]) of bilateral inferior arcuate sulci were activated. The regions around the right principal sulcus (area 9/46V) and right superior arcuate sulcus (area 8B) were also significantly activated. Area 9/46V ($x = -16$, $y = 13$, $z = 8$, $T = 4.19$, $p < 0.001$, FDR corrected) and area 8B ($x = -15$, $y = 8$, $z = 15$, $T = 3.10$, $p < 0.01$, FDR corrected) were also significantly activated on the contralateral side, although the activation peak was located outside of these regions. In MTL regions, bilateral posterior

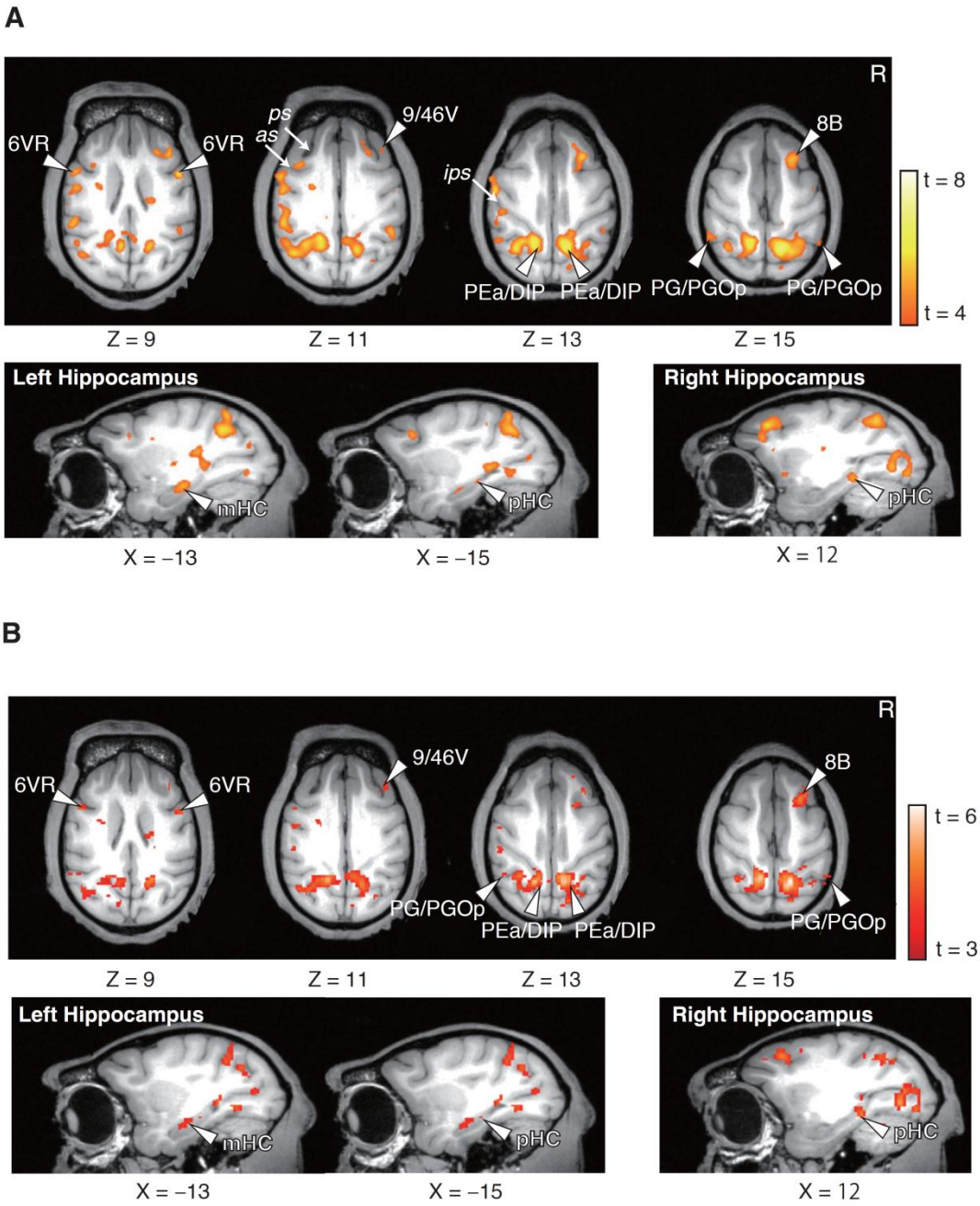

Figure 3. Memory Retrieval Regions in Macaque Cortex

(A) Activation maps (Hit > CR contrast) superimposed on transverse sections (upper panels) and sagittal sections (lower panels) ($t > 4.0$, $p < 0.001$, fixed effect, corrected by FDR). 6VR, ventral premotor; 9/46V, area 9/46V; PEa/DIP, area in intraparietal sulcus; 8B, area 8B; PG/PGOp, area in posterior inferior parietal lobule; mHC, middle hippocampus; pHC, posterior hippocampus; as, arcuate sulcus; ps, principal sulcus; ips, intraparietal sulcus.

(B) Conjunction analysis map. The map of the voxels significantly activated in both monkeys with Hit > CR contrast is shown (conjunction null, $p < 0.05$, corrected by FDR). Conventions are the same as in (A).

Table 1 Abbreviations for memory-related areas

23	area 23
PG/PGOp	parietal area PG/parietal area PG, opercular part
PECg	parietal area PE, cingulate part
PEa/DIP	parietal area PEa/depth intraparietal area
PEa	parietal area PEa
PF/PFOp	parietal area PF/parietal area PF, opercular part
2	area 2
mHC	middle hippocampus
pHC	posterior hippocampus
8B	area 8B
44	area 44
45B	area 45B
9/46V	area 9/46, ventral part
6/32	area 6/32
6M	area 6, medial part
6VR (F5)	area 6, ventral part, rostral subdivision
IPa	intraparietal sulcus associated area in the superior temporal sulcus
Tpt	temporoparietal area
ST1	superior temporal sulcus area 1
ST3	superior temporal sulcus area 3
AI	agranular insular cortex
DI	dysgranular insular cortex
V2	visual area 2
V4	visual area 4
PO	parieto-occipital area
V4D	visual area 4, dorsal part
V4A	visual area 4A
AcbC	accumbens nucleus, core
Pu	Putamen
Cd	caudate nucleus
SN	substantia nigra
HC	hippocampus
PRC	perirhinal cortex
cERC	caudal entorhinal cortex

Abbreviations for retrieval- and encoding- related areas in macaque monkeys. The nomenclature of areas is based on the atlas of Paxinos et al.[24].

Table 2 Brain regions activated in Hit > CR contrast

Hemisphere	Coordinates (mm)			t value	Area	Module
	x	y	z			
Parietal cortex						
L	-4	-26	8	5.6	23	2
L	-22	-20	16	4.1	PG/PGOp	2
R	21	-24	15	4.5		2
R	6	-18	16	3.9	PECg	2
L	-7	-25	13	6.3	PEa/DIP	3
R	6	-26	14	7.1		3
L	-10	-18	18	5.4	PEa	3
R	24	-10	5	4.4	PF/PFOp	4
L	-24	-9	10	4.1		4
L	-22	-3	11	5.2	2	4
Hippocampus						
L	-13	-12	-7	5.4	mHC	1
R	12	-20	-5	5.0	pHC	1
L	-15	-17	-5	4.0		1
Frontal cortex						
R	11	10	14	5.8	8B	2
L	-16	3	6	3.5	44	3
L	-16	7	10	4.7	45B	3
R	11	8	6	4.2		3
R	16	12	9	5.0	9/46V	3
L	-6	-4	17	5.2	6/32	3
L	-3	3	19	4.3	6M	3
L	-23	2	11	5.2	6VR(F5)	4
R	20	3	8	5.7		4
Temporal cortex						
L	-17	-7	-11	3.7	IPa	2
L	-22	-16	10	5.0	Tpt	2
R	20	-20	11	5.6		2
L	-22	2	-10	5.1	ST1	6
L	-25	-3	-2	3.5	ST3	4
Insular cortex						
R	15	3	-3	3.4	AI	4
L	-19	2	-1	5.1	DI	4
R	21	1	1	4.7		4
Occipital cortex						
R	10	-32	-3	4.2	V2	5
L	-12	-33	-3	5.1		5
R	10	-38	-3	5.1	V2	5
L	-16	-33	4	3.6	V2	5
R	2	-40	3	4.9	V2	5
R	7	-33	5	4.6	V2	5
L	-4	-35	8	3.9		5
L	-26	-24	5	4.6	V4	5
R	5	-28	6	4.7	PO	5
L	-18	-29	11	5.7	V4D	5
L	-14	-26	12	5.9	V4A	5
Subcortical						
L	-9	4	-2	3.9	AcbC	2
L	-9	-11	0	4.4	Thalamus	4
R	12	-8	5	3.8	Pu	4
L	-12	-2	10	5.0	Cd	4
R	6	-13	-5	4.7	SN	6
L	-14	-19	1	4.5	Cd	6

Significant peaks at a voxel level of $p < 0.01$ corrected for multiple comparisons. Coordinates are listed in monkey bicommissural space [2, 4]. The abbreviations for the areas are provided in Table 1.

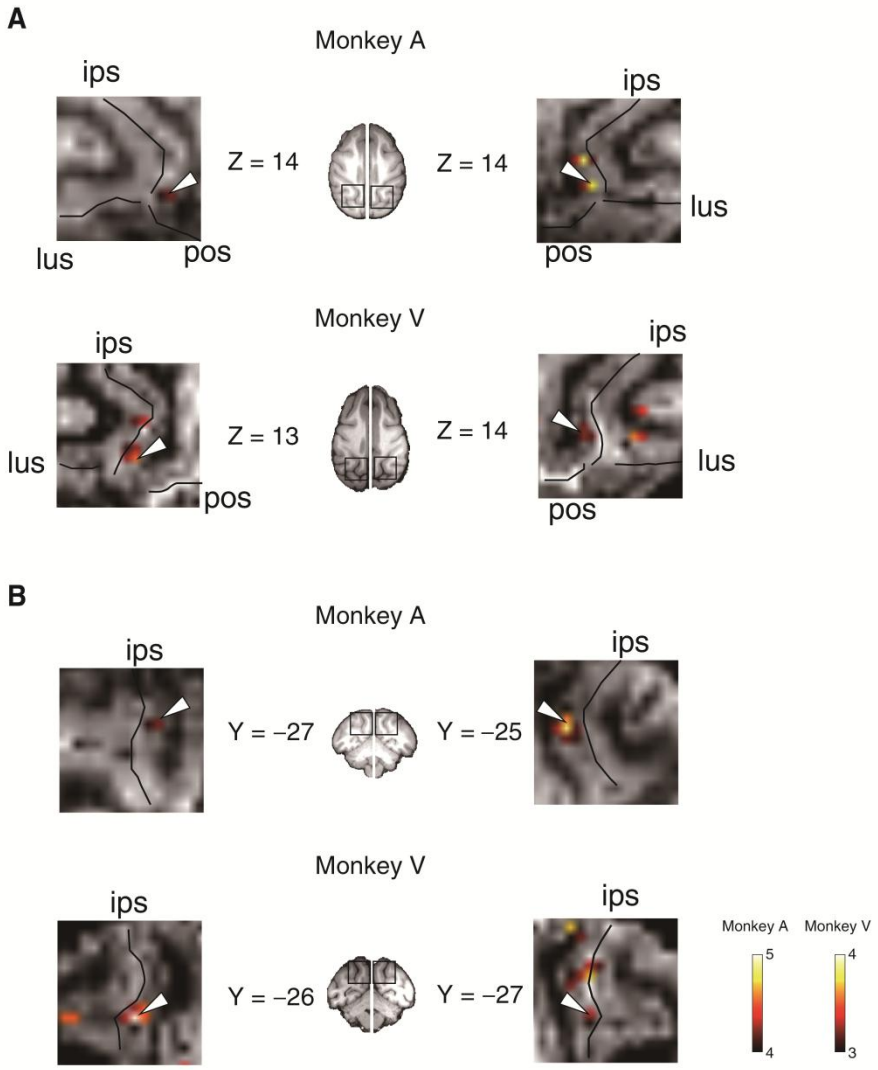

Figure 4. Localization of activation peak on the medial bank of intraparietal sulcus
The activation peaks obtained from GLM analysis by using functional images without spatial smoothing. Activation sites are overlaid on individual EPI images of Monkey A and V. Regions adjacent to PEa/DIP are magnified and displayed on both the axial (A) and the coronal (B) planes. Activation peaks corresponding with PEa/DIP are indicated by arrows. Lines in magnified images indicate sulcui. ips, intraparietal sulcus; lus, lunate sulcus; pos, parieto-occipital sulcus. To display the location of individual activation peaks optimally, the threshold of activation is adjusted in each monkey.

hippocampi (pHC) and left middle hippocampus (mHC) were strongly activated. The right mHC was also activated (x = -16, y = -15, z = -9, T = 3.34, $p < 0.01$, FDR corrected), although the activation peak was located outside of this region. Figure 3B shows the regions that were significantly activated in both of the monkeys for Hit vs. CR (conjunction null, $p < 0.05$, FDR corrected) [25, 26]. This conjunction analysis showed that the majority of activated spots, especially in the parietal cortex, frontal cortex, and hippocampus, were duplicated in individual monkeys.

Neural correlates of the primacy and recency effects in retrieval-related regions

Next we examined if retrieval activities in the identified regions changed depending on the position of the cue item during the serial probe recognition task. To characterize retrieval-related activities in PPC, we first focused on the IPL (PG/PGOp) and the IPS (PEa/DIP), as well as the hippocampi (pHC, mHC) that were suggested to be related to the primacy effect in previous human studies [45]. We examined the effect of cue item position on the retrieval-related activities in each region by conducting an across-session repeated-measures multivariate ANOVA (MANOVA; four levels of retrieved cue item positions × two hemispheres × two monkeys). For the regions where MANOVA showed a significant main effect of retrieved cue item positions without significant interaction with either hemisphere or monkey, we then conducted regression analyses using a "primacy predictor" (n_p) and a "recency predictor" (n_r). In the bilateral hippocampi, MANOVA showed a significant main effect of retrieved cue item position ($F(3,22) = 3,60$, $p=0.03$) for the retrieval activity, and the regression analyses revealed significant positive modulation to the first items ($\beta_p = 0.58 \pm 0.13$ [mean±SEM], $t(51) = 4.24$, $p<0.001$) with significant negative modulation to the last items ($\beta_r = -0.53 \pm 0.15$, $t(51) = -3.45$, p

= 0.002) (Figures 5A, D, E). Also in the bilateral PG/PGOp, MANOVA showed a main effect of retrieved cue item position (F(3,22) = 3.25, p = 0.04), and significant positive modulation was observed in response to the initial items (β_p = 0.59±0.16, t(51) = 3.64, p = 0.001) but not to the last items (β_r = -0.35±0.15, F(1,24) = -2.22, p = 0.06) (Figures 5B, D, E). In the bilateral PEa/DIP, MANOVA showed a main effect of retrieved cue item position (F(3,22) = 3.26, p = 0.04). By contrast with hippocampi and PG/PGOp, significant positive modulation was observed in response to the last items (β_r = 0.33±0.13, t(51) = 2.46, p = 0.03) but not to the initial items (β_p = 0.22±0.15, t(51) = 1.43, p = 0.31) (Figures 5C, D, E). I also confirmed that the hippocampus and PG/PGop were activated for successful retrieval of the initial items (Hit1) compared to correct identification of previously unseen items (CR) during the serial probe recognition task. These results indicate that retrieval-related activity in hippocampi and PG/PGOp reflected the primacy effect, whereas that of PEa/DIP reflected the recency effect.

For the PG/PGOp and PEa/DIP, "serial position effect"-related modulation were also evaluated in consideration of a U-shaped response profile curve. Again, the bilateral PG/PGOp showed significant positive modulation in response to the initial items (β_{up} = 0.40±0.12, t(51) = 3.32, p = 0.001) but not to the last items (β_r = -0.13±0.11, t(51) = -1.11, p = 0.26). On the other hand, the bilateral PEa/DIP showed significant positive modulation in response to the initial items (β_{ur} = 0.34±0.10, t(51) = 3.15, p = 0.002) as well as to the last items (β_{up} = 0.28±0.12, t(51) = 2.25, p = 0.02). These results suggested another possibility that the retrieval-related activity of PEa/DIP reflects not only the recency effect but also the behavioral performance during the task.

Differential increase in effective connectivity during retrieval

To investigate whether the retrieved cue item position affects not only their activity but also the

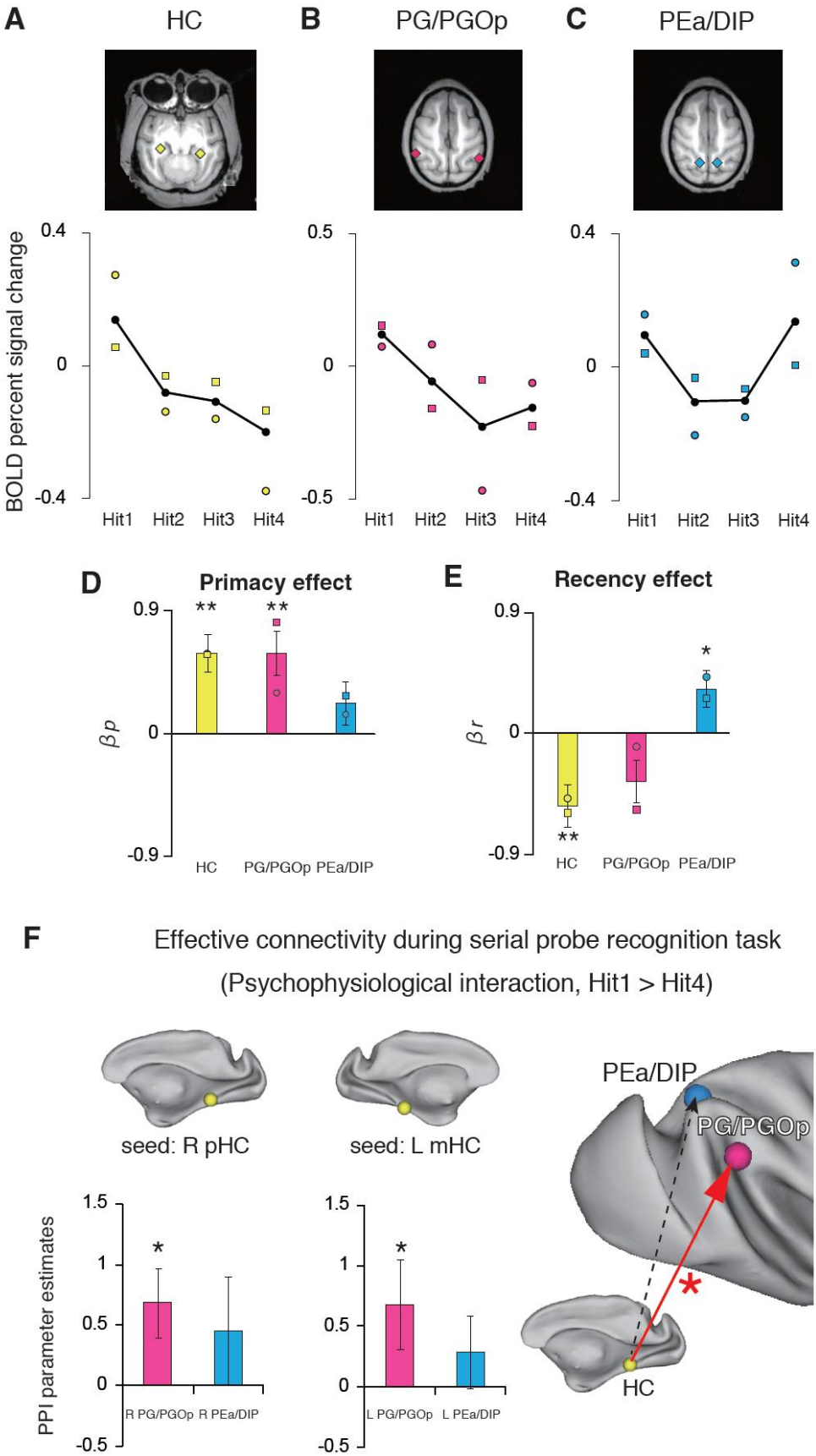
A
HC
B
PG/PGOp
C
PEa/DIP
BOLD percent signal change
0.4
0
-0.4
0.5
-0.5
Hit1
Hit2
Hit3
Hit4
D
Primacy effect
E
Recency effect
0.9
-0.9
βp
βr
**
*
HC
PG/PGOp
PEa/DIP
F
Effective connectivity during serial probe recognition task
(Psychophysiological interaction, Hit1 > Hit4)
seed: R pHC
seed: L mHC
PEa/DIP
PG/PGOp
HC
PPI parameter estimates
1.5
1
0.5
R PG/PGOp
R PEa/DIP
L PG/PGOp
L PEa/DIP

Figure 5. BOLD Signal Changes and Task-evoked Connectivity during Retrieval in the Serial Probe Recognition Task.

(A-C) BOLD percent signal changes in the Hit trials compared with those in the CR trials (Hit vs. CR). Abscissa, four types of Hit trials (Hit1–Hit4) classified according to retrieved cue item position. (A) hippocampus (HC; right pHC and left mHC). (B) posterior inferior parietal lobule (bilateral PG/PGOp). (C) intraparietal sulcus (bilateral PEa/DIP). Each square and circle represents the average signal change from Monkey A and Monkey V, respectively.

(D-E) Comparisons of β coefficient calculated by regression analyses. Abscissa, three regions in (A) to (C). (D) β coefficient for primacy effect (β_p). (E) β coefficient for recency effect (β_r). * $p < 0.05$, ** $p < 0.01$ with Bonferroni correction. Each square and circle represents the β coefficient for Monkey A and Monkey V, respectively. Error bars: SEM across sessions.

(F) Psychophysiological interactions (PPI) in the serial probe recognition task. The left panel shows the couplings between the right posterior hippocampus (pHC) and the two PPC subregions (right PG/PGOp and right PEa/DIP) in retrieval of the initial item (Hit1) after subtraction of those in retrieval of the last item (Hit4). The asterisks indicate significant increase in effective connectivity ($p < 0.05$, FWE corrected within each region). Error bars: SEM. Middle panel shows the results of PPI analysis of effective connectivity from the left middle hippocampus (mHC) to the left PG/PGOp and left PEa/DIP. The right panel shows a scheme of effective connectivity from hippocampus to parietal regions (PG/PGOp, PEa/DIP). Red arrow with asterisk: significant positive effective connectivity. Black dotted arrow: non-significant effective connectivity.

connectivity among these three retrieval-related regions, we conducted a psychophysiological interaction (PPI) analysis. When we located the PPI seed on the right pHC, comparisons of the retrieval of the initial items against that of the last items led to significantly increased effective connectivity with the right PG/PGOp ($p = 0.01$, family-wise error [FWE] corrected within PG/PGOp) but not with the right PEa/DIP ($p > 0.05$, FWE corrected) (Figure 5F, left panel). These results suggested that the right PG/PGOp connected more strongly with right pHC when the right pHC was highly activated for retrieval of the initial item than for retrieval of the last item. The same results were replicated in the left hemisphere (Figure 5F, middle panel): when the PPI seed was located on the left mHC, the retrieval of the initial item against the last led to significantly increased functional connectivity with the left PG/PGOp ($p = 0.04$, FWE corrected) but not with the left PEa/DIP ($p > 0.05$, FWE corrected). Thus, stronger functional connection from the hippocampus to the posterior IPL (PG/PGOp) during the retrieval of the initial cue item was replicated in both hemispheres (Figure 5F, right panel).

We also conducted effective connectivity analyses from retrieval-related areas in PPC, either PEa/DIP or PG/PGOp, to that in earlier visual areas (V4) (Figure 6). In the PPI analyses from the two PPC sites to V4 (Hit4 > Hit2), PEa/DIP showed a significantly positive PPI during a serial probe recognition task ($p < 0.001$, FWE corrected, small volume correction for V4), while PG/PGOp did not ($p > 0.05$, FWE corrected).

Cortical network modules of retrieval-related regions

The above findings implied functional dissociation between IPL (PG/PGOp) and medial IPS (PEa/DIP). To further confirm this difference at the brain-wide network level, we first compared the anatomical connection maps of the two PPC sites, IPL (red, Figure 7A, left) and medial IPS

A Identification of V4 retrieval area related to top-down attentional network
(Retrieval-related activity: Hit > CR and Psychophysiological interaction: Hit 4 > Hit 2)

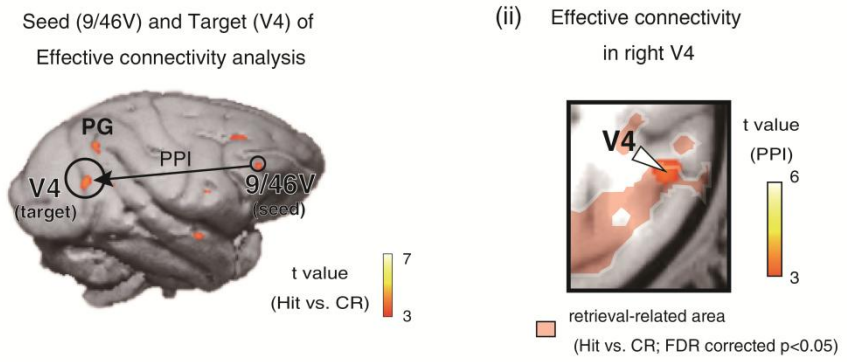

B

Effective connectivity during serial probe recognition task
(Psychophysiological interaction, Hit 4 > Hit 2)

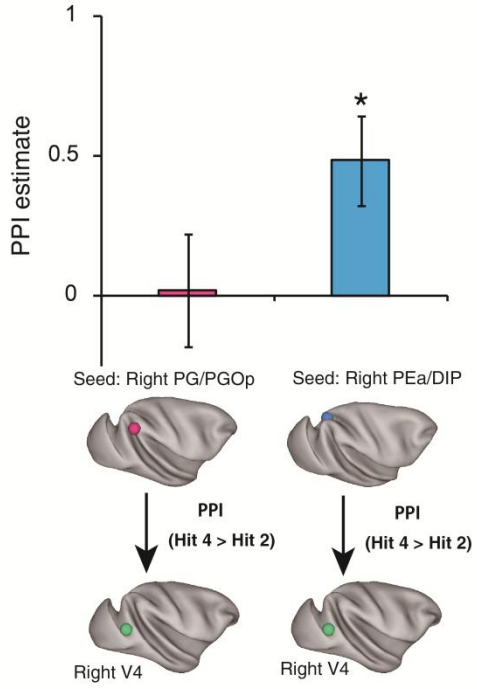

C

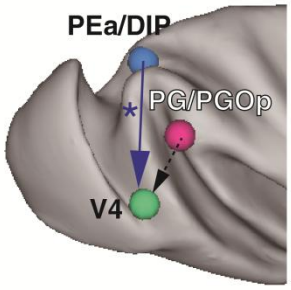

Figure 6 Task-evoked connectivity from PPC to visual area (V4) during memory retrieval
(A) Identification of the target region for PPI.
(i) Seed (right 9/46V) and target regions (right V4) of PPI for target localization. These areas are indicated on the surface of 3D-rendered brain image of Monkey A. Activation map (colored) was superimposed in the contrast Hit vs. CR in the single-probe task.
(ii) Effective connectivity in the right V4. Color t-value map of PPI (Hit4 > Hit2, in the serial probe recognition task) was overlaid on the magnified axial image. The arrow head indicates peak site in area V4. Magenta map was superimposed, indicating the retrieval-related area (Hit vs. CR, $p<0.05$ FDR corrected). Color scale indicates t-value of PPI analysis.
(B) Psychophysiological interactions (PPI) from PPC to V4 in the serial probe recognition task. The couplings between the two PPC subregions (right PG/PGOp [pink] and right PEa/DIP [light blue]) and the right V4 in the retrieval of the last item (Hit 4) after subtraction of those in retrieval of the second item (Hit2) are shown. The asterisk indicates significant increase in effective connectivity ($p<0.05$, FWE corrected within right V4 region). Error bars: SEM across sessions.
(C) A scheme of effective connectivity from PEa/DIP to V4, not from PG/PGOp to V4. Blue arrow with asterisk: significant positive effective connectivity. Black dotted arrow: non-significant effective connectivity.

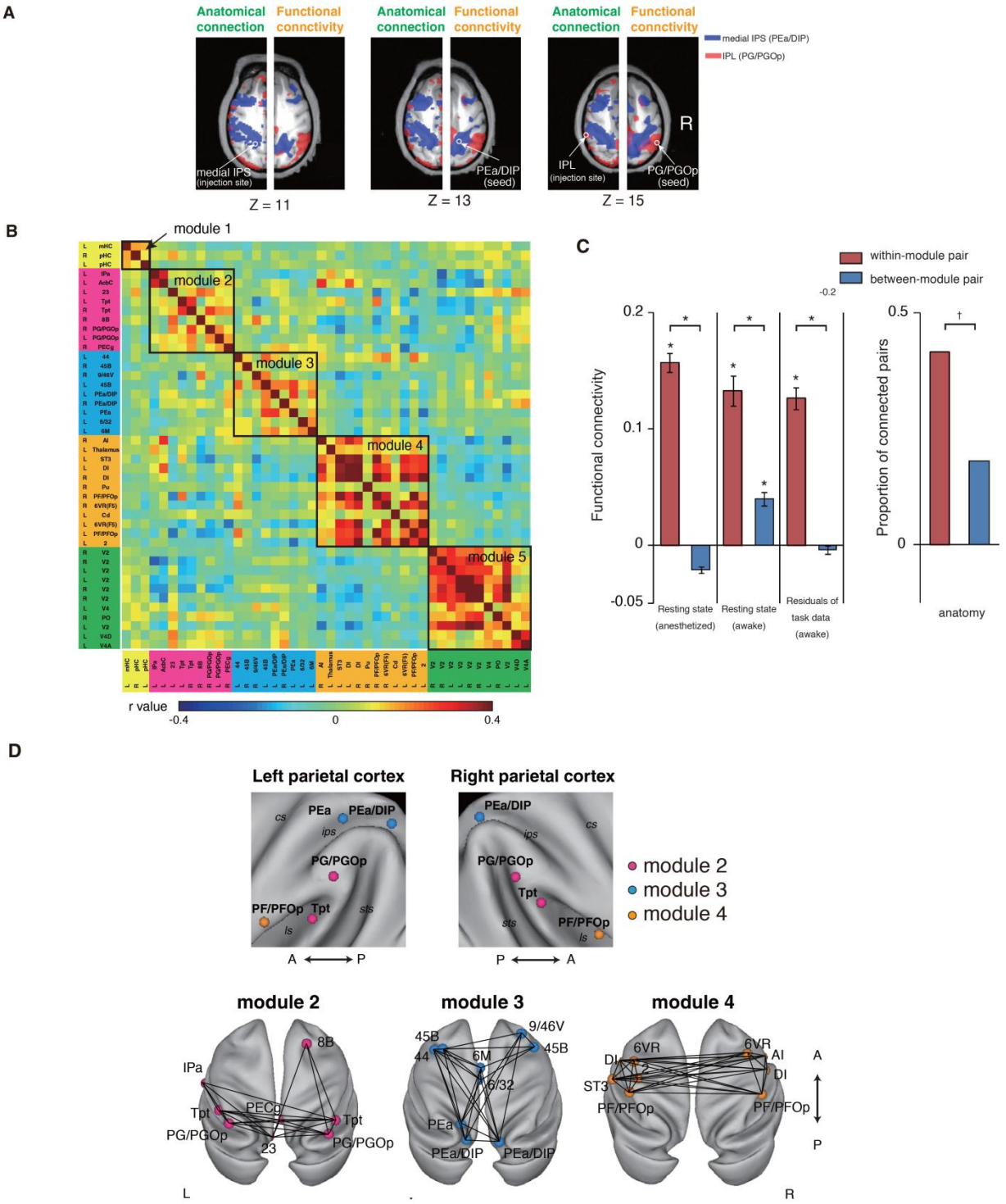
A
Anatomical connection
Functional connctivity
medial IPS (PEa/DIP)
IPL (PG/PGOp)
medial IPS (injection site)
PEa/DIP (seed)
IPL (injection site)
PG/PGOp (seed)
R
Z = 11
Z = 13
Z = 15
B
module 1
module 2
module 3
module 4
module 5
r value
-0.4
0
0.4
C
within-module pair
between-module pair
Functional connectivity
Proportion of connected pairs
Resting state (anesthetized)
Resting state (awake)
Residuals of task data (awake)
anatomy
D
Left parietal cortex
Right parietal cortex
PEa
PEa/DIP
PG/PGOp
PF/PFOp
Tpt
cs
ips
sts
ls
A
P
module 2
module 3
module 4
IPa
8B
PECg
23
45B
44
9/46V
6M
6/32
6VR
AI
DI
ST3
L
R

Figure 7 Five Modules of Retrieval Network Identified by Modularity Optimization

(A) Anatomical connection and functional connectivity maps. Left half in each panel: anatomical connection maps obtained from the data of tracer injection in Lewis and Van Essen (2000). Small circles indicate the location of injection sites (IPL, red, Case D; medial IPS, blue, Case A). Right half in each panel: voxel-wise map of spontaneous BOLD functional connectivity (BOLD-FC) obtained with the seed regions at the right PG/PGOp (red) and at the right PEa/DIP (blue). Small circles indicate the location of seed regions. Maps are thresholded at $r > 0.12$.

(B) BOLD-FC matrix among the retrieval-related regions listed in Table 2. Rows and columns indicate the regions sorted by optimized modules. Retrieval-related regions were split into non-overlapping modules, one of which (module 1 [yellow]) consisted of hippocampus, three of which (module 2 [pink], module 3 [light blue], module 4 [orange]) contained regions within the PPC, and one of which (module 5 [green]) consisted of regions in the occipital cortex.

(C) Left panels: comparisons of functional connectivity between within- (red) and between-module (blue) pair of retrieval-related areas from the data of the resting state experiment of the anesthetized monkeys (left), the data of the resting state experiment of the awake monkeys (middle), and the data from the analysis of residual timecourses of the awake task experiment (right). *: $p < 0.001$. Right panel: comparisons of proportion of anatomically connected pairs between within- and between-module pair of retrieval-related areas. Error bars: SEM across regions. †: $p < 0.001$ (chi-square test).

(D) Spatial configurations of the retrieval-related modules in the macaque cortex. Modules are displayed on the inflated cortical surface using Caret software. Upper panels show module assignments in PPC. cs, central sulcus; ips, intraparietal sulcus; ls, lateral sulcus; sts, superior temporal sulcus. Lower panels show all the cortical regions in the three modules containing PPC regions (module 2, 3, 4). Pairs of regions in each module with significant BOLD-FC are interconnected with lines ($p < 0.05$, Bonferroni correction by the number of combinations among all the retrieval-related regions).

(blue, Figure7A, left). The overlap between these two anatomical connection maps was marginal. Next we calculated the functional connectivity map of spontaneous BOLD activity under anesthesia (Figure 7A, right). The functional connectivity map for seed regions of PG/PGOp (red, Figure 7A, right) covered the lateral parietal cortex and posterior cingulate cortex, while the map for PEa/DIP (blue, Figure 7A, right) covered the principal, arcuate, and intraparietal sulci. The overlap between these functional connectivity maps was also marginal. Moreover, the anatomical connection maps were in close agreement with functional connectivity maps. Then we evaluated the anatomical and functional connection patterns of the two PPC sites in whole brain (Figure 8A) with the aid of CoCoMac database (collection of past tracer studies in the macaque cerebral cortex) [40]. As reported previously [21], the strengths of anatomical connections were significantly correlated with the functional connectivities (PG/PGOp: $r = 0.45$; $p < 0.001$; PEa/DIP: $r=0.42$, $p=0.002$) (Figures 8C and D). From multiple regression analyses, functional connectivity with PG/PGOp is significantly correlated with the strength of axonal projections with PG/PGOp ($p < 0.001$) but not with PEa/DIP ($p > 0.05$) (Figure 8E, left panel). On the other hand, functional connectivity with PEa/DIP is significantly correlated with the strength of axonal projections with PEa/DIP ($p < 0.001$) but not with PG/PGOp ($p > 0.05$) (Figure 8E, right panel). These results suggested that the anatomical connection patterns of the two PPC sites are dissociated enough to separately predict functional connectivity with the two PPC sites, respectively (Figures 8C, D, E). In addition, we compared the anatomical connection and functional connectivities for all combinations of retrieval-related areas. The strengths of anatomical connections were again correlated with the functional connectivity ($r = 0.23$; $p = 0.003$) (Figure 8F).

To objectively segregate the 47 identified retrieval-related regions including PG/PGOp and

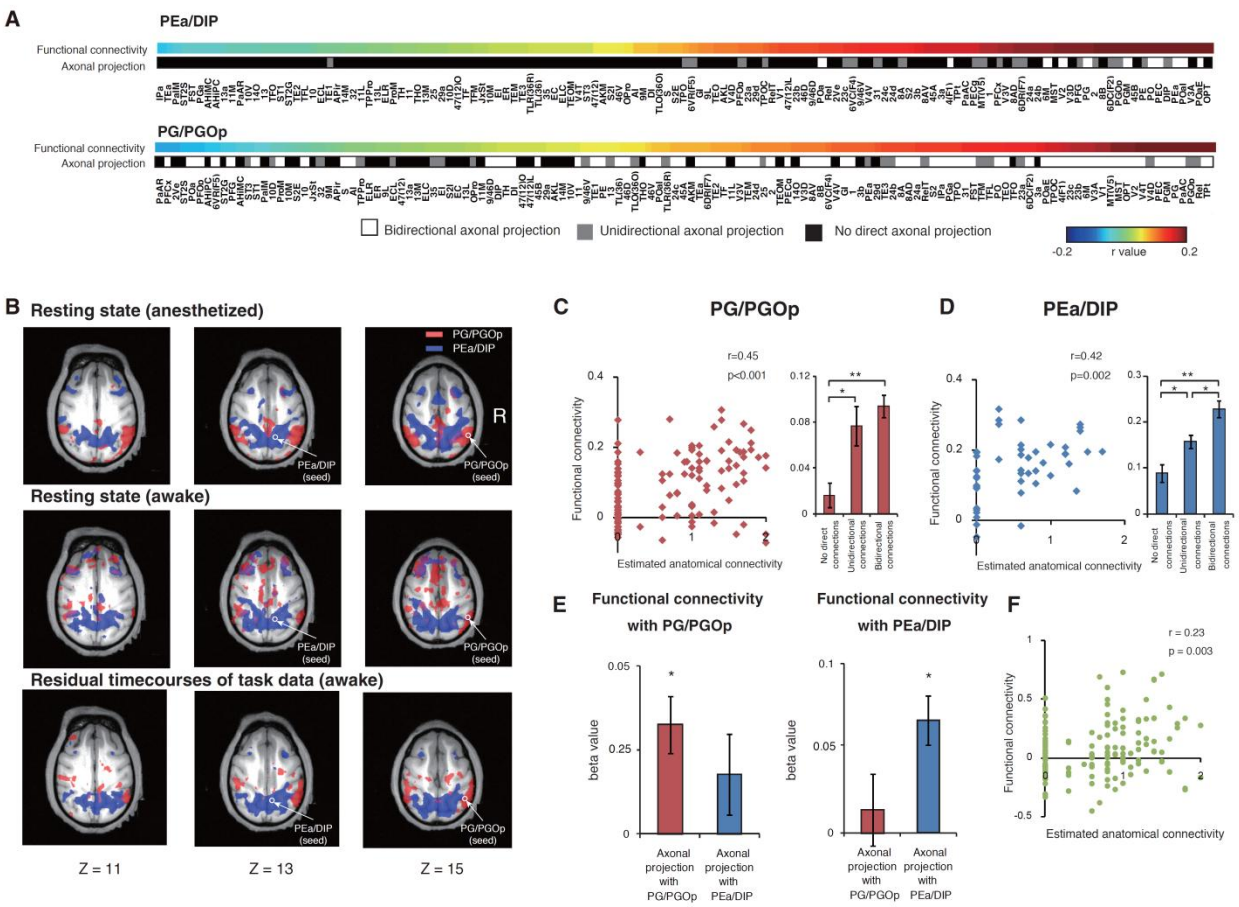

Figure 8. Comparisons of anatomical and functional connectivity networks of retrieval-related areas

(A) Anatomical and functional connection patterns of PEa/DIP and PG/PGOp in whole brain shown in Figure 4B, with area name information.

(B) Voxel-wise map of spontaneous BOLD functional connectivity (BOLD-FC) obtained with the seed regions at the right PG/PGOp (red) and the right PEa/DIP (blue). Upper panels show the functional connectivity maps from the resting state experiment under anesthesia. Middle panels show the functional connectivity maps from the resting state experiment in the awake condition. Lower panels show the functional connectivity maps from the data of residual timecourses of awake task data. Small circles indicate the location of seed regions. Maps are thresholded at $r > 0.12$ for anesthesia and residual timecourses, and at $r > 0.2$ for awake.

(C, D) Relationship between functional connectivity and anatomical connections with PG/PGOp (C) or PEa/DIP (D). Left panels show the scatter plot of estimated anatomical connectivity based on CoCoMac database (abscissa) and functional connectivity (Fisher's z transformed correlation coefficients) (ordinate) from PG/PGOp (C, red) or PEa/DIP (D, blue) to other regions, with which anatomical connection has been described in previous literature. Right panels show the comparisons of functional connectivity among area pairs that have bidirectional, unidirectional, and no axonal projections. *: $p < 0.01$. **: $p < 0.001$. Error bars: SEM across regions.

(E) Comparisons of β coefficient for the functional connectivity with PG/PGOp or PEa/DIP calculated by multiple regression analyses. As predictors of this regression analyses, the number of projections between each area and PG/PGOp (0: no direct axonal projections, 1: unidirectional

axonal projection, 2: bidirectional axonal projections) and the number of projections between each area and PEa/DIP were used. *: $p < 0.001$ with Bonferroni correction. Error bars: SEM across regions.

(F) Scattergram showing estimated anatomical connectivity (abscissa) and functional connectivity (Fisher's z transformed correlation coefficients) (ordinate) for each region that include retrieval-related activations.

PEa/DIP, we conducted community detection analysis using modularity optimization of the functional connectivity of spontaneous BOLD activity under anesthesia from the same monkeys as the recognition memory experiments [42]. We configured a matrix of pair-wise functional connectivity correlations between each of the 47 regions (Figure 7B). Modularity optimization separated the regions into six distinct groups, or modules (modularity measure Q = 0.59), where PG/PGOp and PEa/DIP were classified separately. This Q value indicated strong community structure that exceeded the criterion adopted by previous studies, 0.30 [41, 46]. Module 1 consisted of bilateral hippocampi. Module 2 (pink, Figure 7D) contained bilateral PG/PGOp, temporoparietal areas (Tpt), posterior cingulate cortices (area 23, PECg), and right area 8B. These regions were included among the areas that demonstrated high functional connectivity to the seed region of PG/PGOp (red, Figure 7A). Module 3 (light blue, Figure 7D) contained bilateral PEa/DIP, area 45B, and right area 9/46V. These regions were included among the areas that demonstrated high functional connectivity to the seed region of PEa/DIP (blue, Figure 7A). These results confirmed that the two parietal retrieval-related regions, PG/PGOp and PEa/DIP, are involved in separate retrieval-related networks. Module 4 (orange, Figure 7D) contained bilateral 6VR, insula, and anterior IPL (PF/PFOp). Module 5 covered all regions in occipital cortex. Module 6 was excluded from later analysis because two of the three regions belonged to subcortical areas. The fact that retrieval-related regions in PPC participated in three (modules 2, 3, 4) of the six modules (Figure 7D, upper panel) suggests that the different modules of a brain-wide memory-retrieval network coexist in PPC.

Resting state data in the awake condition was also collected from the same two monkeys (Figure 8B). We confirmed that the modular structure extracted from spontaneous BOLD activity in anesthetized monkeys was preserved in awake monkeys ($p < 0.001$ for each) (Figure 7C, left

panels). We also confirmed that the proportion of anatomically connected pairs of areas within the same module was significantly higher than pairs from different modules ($p < 0.001$) (Figure 7C, right panel). Thus, the modular structures extracted from the functional connectivity networks reflected the anatomical structures of the retrieval-related networks.

Cortical network reflecting the primacy and recency effects

Finally, we examined whether population activity within each of the separated modules above reflects the primacy or recency effects. For module 1, MANOVA (four levels of retrieved cue item positions × regions within the module × two monkeys) yielded a significant main effect of retrieved cue item position ($F(3,22) = 3.67$, $p = 0.02$) on normalized BOLD signals (see Materials and Methods) with no interactions with the level of region ($F(6,19) = 1.91$, $p = 0.13$) or monkey ($F(3,22) = 0.46$, $p > 0.5$) (Figure 9A). For module 2, MANOVA yielded a significant main effect of retrieved cue item position ($F(3,22) = 3.80$, $p = 0.02$) with no interactions with the level of region ($F(24,1) = 0.30$, $p > 0.5$) or monkey ($F(3,22) = 0.20$, $p > 0.5$) (Figure 9B). For module 3, MANOVA yielded a significant main effect of retrieved cue item position ($F(3,22) = 4.37$, $p=0.01$) with no interactions with the level of region ($F(24,1) = 0.24$, $p > 0.5$) or monkey ($F(3,22) = 1.62$, $p = 0.21$) (Figure 9C). Modules 4 and 5 did not demonstrate any significant main effects of retrieved cue item position (all $p > 0.05$) (Figures 9D, E).

For modules 1 to 3, which demonstrated a main effect of retrieved cue item position, we conducted regression analyses using a "primacy predictor" (n_p) and "recency predictor" (n_r) for the normalized BOLD signal from Hit1 to Hit4. Module 1 demonstrated significant positive modulation by retrieval of the initial items ($\beta_p = 0.33 \pm 0.12$, $t(77) = 2.80$, $p = 0.01$) with significant negative modulation by retrieval of the last items ($\beta_r = -0.39 \pm 0.12$, $t(77) = -3.05$, $p =$

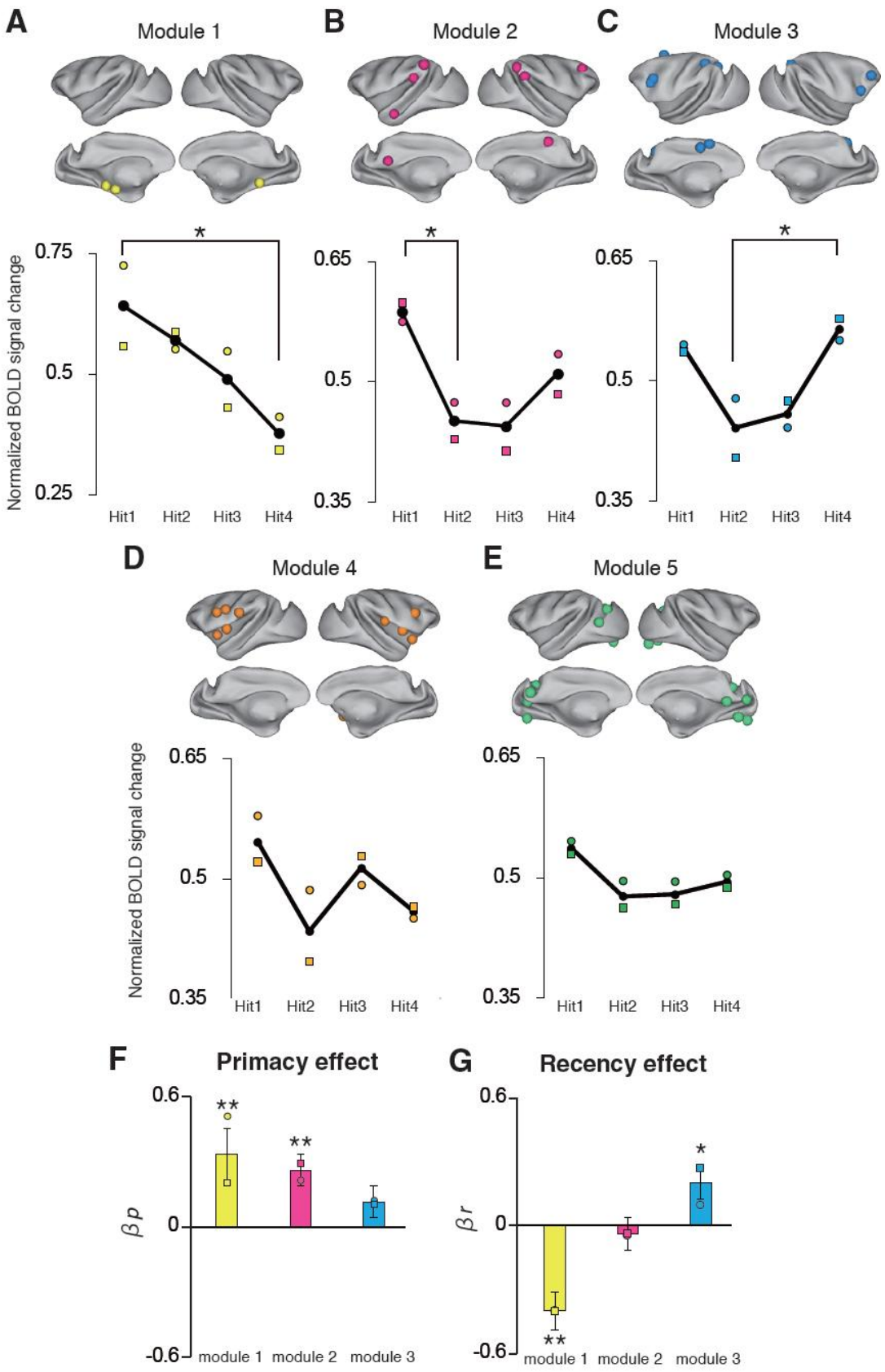
A
Module 1
B
Module 2
C
Module 3
Normalized BOLD signal change
0.75
0.5
0.25
0.65
0.35
Hit1
Hit2
Hit3
Hit4
D
Module 4
E
Module 5
F
Primacy effect
G
Recency effect
βp
βr
0.6
0
-0.6
module 1
module 2
module 3

Figure 9. Primacy Effect and Recency Effect in Retrieval Network Modules

(A) Retrieval-related activity within module 1. Abscissa: the four types of Hit trials (Hit1-Hit4) classified by the retrieved cue item position. Ordinate: Normalized percent signal changes of all the constituent retrieval-related regions in this module. Each square and circle represents the average signal change from Monkey A and Monkey V, respectively. *: $p < 0.05$ (paired t test, Bonferroni corrected). All the regions in module 1 are shown on lateral and medial views of the cortex using Caret software.

(B–E) Same as in (A) but for module 2 (B), module 3 (C), module 4 (D), and module 5 (E).

(F, G) Comparisons of β coefficient calculated by regression analyses. Abscissa, three modules shown significant main effect of the retrieved cue item position in MANOVA (module 1, 2, 3). (F) β coefficient for primacy effect (β_p). (G) β coefficient for recency effect (β_r). *: $p < 0.05$, **: $p < 0.01$ with Bonferroni correction. Each square and circle represents the β coefficient for Monkey A and Monkey V, respectively. Error bars: SEM across sessions.

0.006) (Figures 9A, F, G). Module 2 demonstrated positive modulation by retrieval of the initial items (β_p = 0.26±0.07, t(233) = 3.64, p < 0.001) but no significant modulation by retrieval of the last items (β_r = 0.03±0.07, t(233) = -0.51, p > 0.5) (Figures 9B, F, G). Conversely, module 3 demonstrated significant positive modulation by retrieval of the last items (β_r = 0.19±0.07, t(233) = 2.79, p = 0.01) with no significant modulation by retrieval of the initial items (β_p = 0.11±0.07, t(233) = 1.58, p = 0.22) (Figures 9C, F, G). In summary, the MANOVA and the regression analyses applied here indicate that modules 1 and 2 are involved in retrieval of the initial cue items, which is related to primacy effect, module 3 is involved in retrieval of the last items, which is related to recency effect, and modules 4 and 5 are not affected by retrieved cue item position.

For the modules 2 and 3, "serial position effect"-related modulation were also evaluated in consideration of a U-shaped response profile curve. Again, the module 2 showed significant positive modulation in response to the initial items (β_{up} = 0.21±0.05, t(233) = 3.32, p < 0.001) but not to the last items (β_r = 0.04±0.05, t(233) = 0.72, p = 0.46). On the other hand, the module 3 showed significant positive modulation in response to the initial items (β_{ur} = 0.20±0.05, t(233) = 3.52, p < 0.001) as well as to the last items (β_{up} = 0.15±0.05, t(233) = 2.63, p = 0.009). These results suggested another possibility that the retrieval-related activity of the module 3 reflects not only the recency effect but also the behavioral performance during the task.

Post-hoc multiple comparisons between each pair of cue item positions also confirmed these findings: module 1 was more activated by retrievals of the first item than the last (Hit1 > Hit4, p = 0.01, Bonferroni correction; other pairs p > 0.05), module 2 was more activated by the first item than the second (Hit1 > Hit2, p = 0.03, Bonferroni correction; other pairs p > 0.05), and module 3 was more activated by the last item than the second (Hit4 > Hit2, p = 0.01, Bonferroni

correction; other pairs $p > 0.05$). These results demonstrated that the segregated modules of the retrieval-related network showed differential response characteristics in the retrieval of different cue item positions.

Part II

Encoding-related network in macaque monkeys

Materials and Methods

The same data as in the previous section, which were acquired from the two monkeys performing the single-probe and serial probe recognition tasks, were analyzed in this section.

Multi-voxel classification analysis

To localize the regions that were predictive of subsequent memory performance, the data from the single-probe recognition task were preprocessed using SPM5 software (http://www.fil.ion.ucl.ac.uk/spm). Functional images were realigned, corrected for slice timing, and spatially normalized to the template image by interpolation to a 1 × 1 × 1-mm^3 space, but without any spatial smoothing. The template image was constructed from the high-resolution EPI of each monkey by co-registering it to each monkey's anatomical template MDEFT image arranged in bicommissural space in which the origin was placed at the anterior commissure [2, 4].

Subsequent memory prediction was performed using a multivariate searchlight strategy, which examines the information in the local spatial patterns surrounding each voxel within the search space limited to the MTL [47-53]. Before the analysis, time series during the single-probe recognition and serial probe recognition tasks were separately estimated for "later Hit" and "later Miss" trials in each session using canonical haemodynamic response functions. This multi-voxel classification analysis was achieved by splitting the subsequent memory prediction data into a training set and a test set. The training set was then used to train a linear support vector machine classifier using the LIBSVM (http://www.csie.ntu.edu.tw/~cjlin/libsvm/) implementation. A standard k-fold cross-validation testing regime was used where k was equal to the number of estimated time series. The data from each time series were set aside and used, in turn, as the test data; the remaining data were used as the training data. This method generated k sets for the

linear support vector machine training and test sets that were used to derive an overall classification accuracy from the proportion of correct classification guesses across all k-folds of the cross-validation. This procedure was repeated for each searchlight sphere (radius = 2 mm), thereby generating a percentage accuracy value for every single voxel within the search space. From the map derived for each monkey, the peaks showing the highest classification accuracy values (listed in Table 3) were extracted and labeled by referring to the atlas of Paxinos et al. [24] and the nomenclature of the 'parahippocampal region' as described below. For the serial-probe recognition task data, classification performance was calculated separately for initial items (Cue1) and middle items (Cue2, Cue3) using the k-fold cross-validation. Two-way ANOVA was performed on the classification accuracy data after arcsine transformation with the factors of position (initial, middle) and area (2-mm radius sphere around bilateral peaks [listed in Table 3] within the hippocampus, cERC, and PRC derived from the multi-voxel classification analysis for the single-probe recognition task. Classification accuracies calculated in each hemisphere were averaged.).

Univariate analysis

The encoding success regions were identified by performing voxel-wise general linear model (GLM) analyses in SPM5. These analyses included the following predictors: (1–4) the choice onsets in Hit, Correct Rejection (CR), Miss, and FA trials; (5–9) the cue onsets in Hit, CR, Miss, FA, and other (aborted) trials; and (10) the timing of other types of errors. These events were modeled as delta functions, convolved with the canonical hemodynamic response function and its temporal and dispersion derivatives. The six parameters of head motion derived from realignment were also included in the model as covariates of no interest. Data were high-pass

filtered using a cutoff of 32 s.

Group analysis of the fMRI data derived from the two monkeys, preprocessed as above and spatially smoothed with a Gaussian kernel (3 mm full-width at half-maximum), was conducted using a fixed-effect model. Functional images from both monkeys were spatially normalized to the template image derived from Monkey A. Encoding success regions were identified according to the group analysis map (see Figure 10A) for the comparison of blood-oxygen-level dependent (BOLD) signals between the “later Hit” (cue onsets in Hit) and “later Miss” (cue onsets in Miss) trials [54]. The coordinates of the activation peaks within the MTL at which the t value was significant at $p < 0.05$ with false discovery rate (FDR) correction [23] are listed in Table 4.

For the serial probe recognition task, voxel-wise GLM analyses were also conducted and significant activation peaks were searched within each region of interest determined in the GLM analysis for the single-probe recognition task (see Figure 10A). The regions of interest for each pair of bilateral activation peaks within MTL were defined as the significant voxels within a 2-mm radius ($p < 0.05$ with FDR correction). Hit and Miss trials were further classified into three categories according to the position of the test item in the cue sequence: Hit [Initial, Middle, Last] and Miss [Initial, Middle, Last]. To examine the effect of test item position in the cue sequence on the encoding success activity in each homotopic pair of regions of interest listed in Table 4 (the PRC and cERC), BOLD signals were separately compared between the “later Hit” and “later Miss” trials for the initial and middle items in population analysis. Two-way ANOVA was performed on the activation values with the factors of position (initial, middle) and area (3-mm radius sphere around bilateral peaks within cERC and PRC where significant activation [$q < 0.05$, FDR corrected] was observed during the single-probe recognition task).

In addition, we estimated the correlation between accuracy and BOLD signal in the two

regions for the initial and middle items. Atypical sessions, in which task accuracy differed from the average by more than 20%, were omitted. Accuracy and brain activity varied across sessions for each monkey were Z-transformed before the correlation coefficient was calculated.

Anatomy and nomenclature of the 'parahippocampal region'

In the present study, I focused on the 'parahippocampal region', along with the hippocampus in the medial temporal lobe. The parahippocampal region, as is often referred to in previous studies, comprises the perirhinal, parahippocampal, and entorhinal cortices [55, 56]. In monkeys, these areas are situated on the anterior-ventral portion of the medial temporal lobe and surround the amygdala anteriorly and the hippocampus posteriorly [56]. Demarcation of the region in the present study was mostly based on Suzuki and Amaral [57-60].

The monkey perirhinal cortex is situated lateral to the fundus of the rhinal sulcus and extends from the posterior border of the rhinal sulcus on the ventral surface of the temporal lobe to the anterior and the dorsal portion of the rhinal sulcus on the temporal pole. The perhinal cortex has been further subdivided into area 35, which forms a long and narrow strip of cortex in the fundus and lateral bank of the rhinal sulcus, and a larger, more laterally situated area 36 [57-60]. However, there exist controversies over the nomenclature and border of the monkey perirhinal cortex. First, regarding the nomenclature, some investigators define only the area 35 as the perirhinal cortex and distinguish it from the area 36 which is labeled as the ectorhinal cortex [61, 62]. Others have grouped perirhinal (area 35) and entorhinal (area 28) together and referred to it as the rhinal cortex [63, 64]. Here, we referred to both the areas 35 and 36 as the perirhinal cortex and distinguished the perirhinal cortex from the entorhinal cortex [57-60]. Secondly, regarding the border, some researchers concern whether the dorsal or ventral temporal pole

adjacent to the rhinal sulcus should also be considered part of the perirhinal cortex. Here, we included the ventral temporal pole, but excluded the dorsal temporal pole, in terms of anatomical connections and cytoarchitectonic features [57, 65-67].

The entorhinal and parahippocampal cortices in monkeys are located on the parahippocampal gyrus, which is separated from the temporal polar cortex and the inferior temporal area by the rhinal sulcus anteriorly and the occipitotemporal sulcus posteriorly. The entorhinal cortex locates anteriorly in the most sizable part of the parahippocampal gyrus. The entorhinal cortex forming area 28 has further been subdivided into six subdivisions based mainly on cytoarchitectonic criteria [68]. In general, the monkey entorhinal cortex enjoys the least controversy over the location of its borders, compared to the perirhinal and parahippocampal cortices. The monkey parahippocampal cortex locates posteriorly on the parahippocampal gyrus and situated just caudal to both the entorhinal and perirhinal cortex. The cortical area is made up of areas TH and TF defined by cytoarchitectonic features, although a controversy exist over the lateral border of the area TF [59, 60, 66, 67, 69].

In humans, much of the parahippocampal region including the entorhinal, perirhinal, and parahippocampal cortices locates on the parahippocampal gyrus [56, 61]. The parahippocampal gyrus is separated from the temporal neocortex laterally by the often variant collateral and rhinal sulci in humans (see [56] for a large individual variance in configuration of the human collateral and rhinal sulci). If the rhinal sulcus is present, the human perirhinal cortex is located in its fundus and lateral bank, as is the case for nonhuman primates, and in the perirhinal gyrus between the rhinal sulcus and collateral sulcus. Even if the rhinal sulcus is absent, the perirhinal cortex aligns itself with the collateral sulcus and continues posteriorly. Although the human entorhinal cortex (area 28) and parahippocampal cortex (areas TF and TH) are located in the

parahippocampal gyrus, posteriorly and ventrally to the primary olfactory cortex, MRI-based boundary delineation between these cortices has not yet been established in humans.

Results

Behavioral results

In this section, I focused on the encoding processes of initial (cue 1) or middle (cues 2 and 3) cue items, which are considered to be dependent on the long-term memory process [11]. Retrieval of the last items on the list is related to the recency effect and is considered to reflect working memory process rather than long-term memory process. For this reason, we excluded the last item on the list from the analyses. The corrected recognition rate (defined as "Hit rate" – "False Alarm [FA] rate") for each position of the cue item (initial, middle) was significantly positive for both monkeys (chi-square test; $p < 0.05$, for each item for both monkeys), suggesting that the monkeys adequately distinguished seen items from unseen items based on items retrieved from memory. Therefore, the areas that predict subsequent memory performance can be considered as memory traces. The accuracy was significantly higher for the initial list position than for the middle list positions (chi-square test; monkey A: $p = 0.04$; monkey V: $p < 0.001$; Figure 1B).

Decoding memory traces in the monkey MTL using multivariate classification

To localize the neural correlates of the subsequent memory effect in the monkey MTL, I applied the searchlight method, a multivariate decoding technique that is based on a linear support vector machine, to the fMRI signals recorded from the MTL during cue periods in the single-probe recognition task. We generated an accuracy map, in which every cluster in the MTL contained the information about the classification accuracy of the subsequent recognition performance, i.e., whether the monkey remembered (later Hit) or forgot (later Miss) (Figure 10A). In the parahippocampal region, the bilateral accuracy peaks common to both monkeys were located within area 36 of the PRC and within caudal part of the entorhinal cortex (cERC) (Figures 10A,

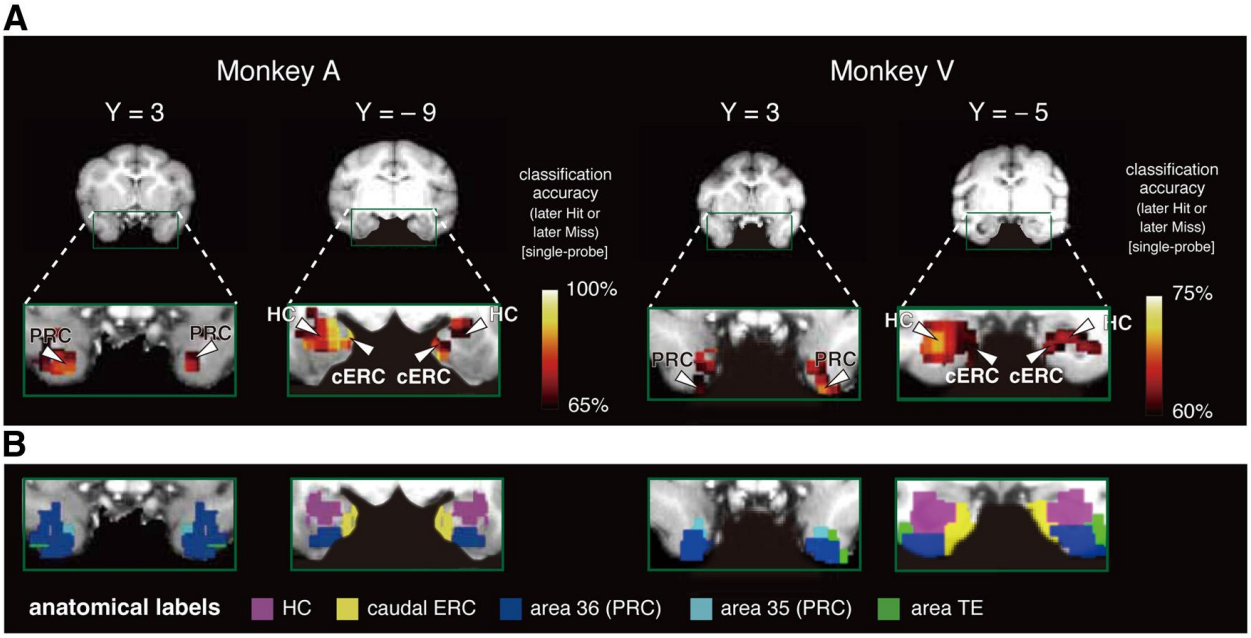

Figure 10. Prediction maps during the single-probe recognition task for each monkey
(A) Prediction maps showing the accuracy of the classification of "later Hit" and "later Miss" trials during single-probe recognition task superimposed on coronal sections. To display the distribution of highly predictable regions in individual monkeys the threshold of activation is adjusted in each monkey.
(B) Anatomical partitioning by Paxinos et al. [24]. HC: hippocampus, PRC: perirhinal cortex, cERC: caudal entorhinal cortex.

B). The pattern of activity in these two cortices and the hippocampus predicted subsequent recognition performance with significantly high accuracy (PRC, monkey A: $p = 6 \times 10^{-9}$, monkey V: $p = 0.003$; cERC, monkey A: $p = 6 \times 10^{-9}$, monkey V: $p = 0.003$; hippocampus, monkey A: $p = 4 \times 10^{-12}$, monkey V: $p = 0.01$; Table 3).

Prediction of subsequent memory performance by the hippocampus, cERC, and PRC activity differentially depends on the list position of the cue item

Next, I examined whether the dependency of decoding accuracy on the position of the cue items in the serial probe recognition task differed across the hippocampus, PRC, and cERC (Figure 11A). Two-way ANOVA (two positions [initial, middle] × three areas) identified a significant interaction between position and area ($F[2,2] = 41.7$, $p = 0.02$), although neither position ($F[1,1] = 57.4$, $p = 0.08$) nor area ($F[1,2] = 0.15$, $p > 0.5$) showed a significant main effect. The three areas were then dissociated to determine their contribution to encoding items in different positions in the cue list. Tests for simple main effects revealed that the decoding accuracy of the cERC ($F[1,3] = 74.4$, $p = 0.003$) and the bilateral hippocampi ($F[1,3] = 16.1$, $p = 0.02$) was significantly higher for initial items than for middle items, whereas the accuracy of the PRC was significantly higher for middle items than for initial items ($F[1,3] = 38.3$, $p = 0.008$). The accuracy maps in the serial probe recognition task which were generated separately for encoding of the initial or middle items jointly overlapped with the accuracy maps from the single-probe recognition task (Figure 11B). These results indicate that the PRC and the cERC along with the hippocampus were engaged in two distinct encoding processes that worked differentially depending on the position of the item in the memorized list.

Table 3 Coordinates of voxels with the highest classification accuracy in the hippocampus (HC), perirhinal cortex (PRC), and caudal entorhinal cortex (cERC) during the single-probe recognition task

Monkey A

		x	y	z	Accuracy
PRC	L	-11	4	-17	85%
	R	11	3	-18	86%
cERC	L	-7	-7	-15	90%
	R	8	-7	-15	89%
HC	L	-11	-17	2	95%
	R	10	-8	-11	97%

Monkey V

		x	y	z	Accuracy
PRC	L	-11	3	-19	61%
	R	11	3	-19	69%
cERC	L	-6	-2	-16	66%
	R	6	-5	-14	62%
HC	L	-14	-5	-12	69%
	R	14	-4	-13	64%

L = left; R = right.

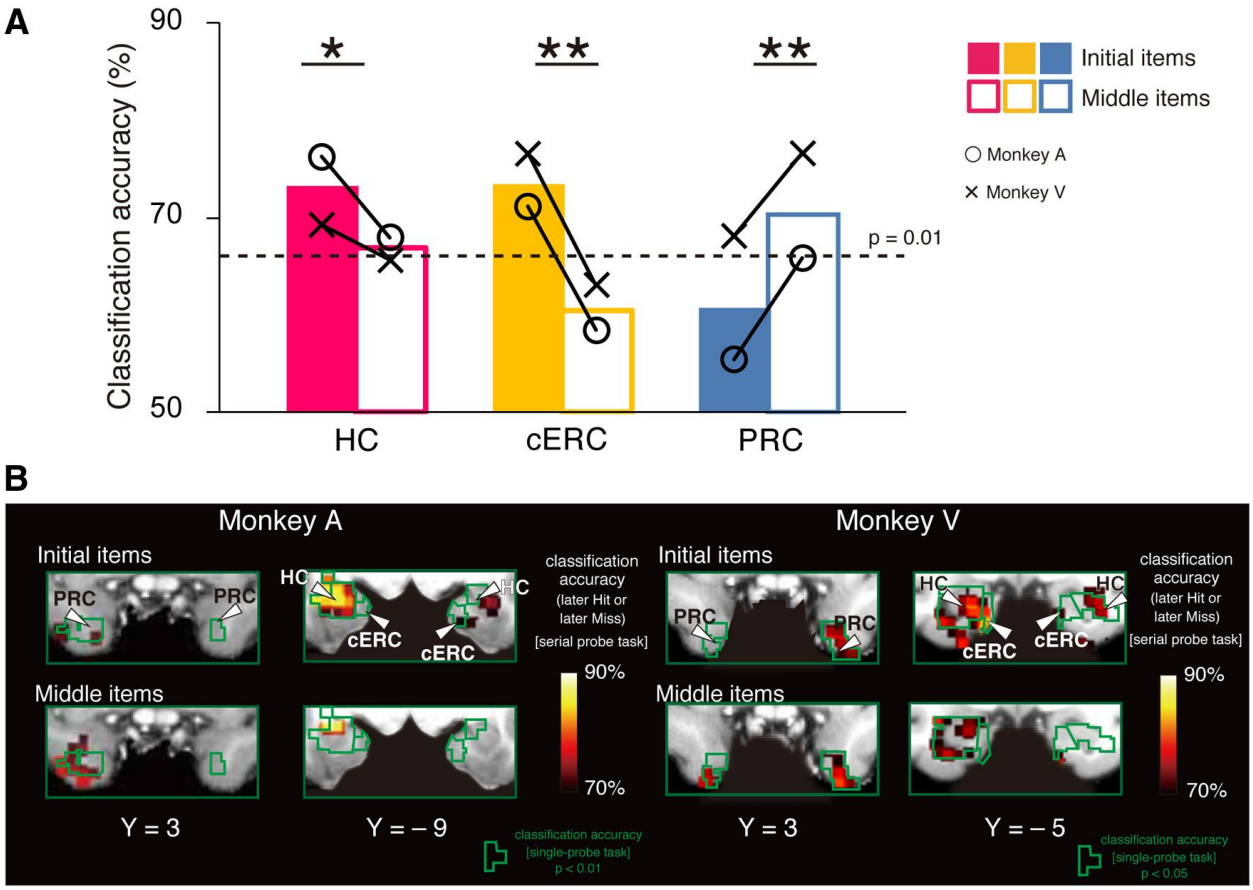

Figure 11. Differential predictability of subsequent memory performance according to multi-voxel classification.

(A) Classification accuracy of the initial (filled bars) and middle (open bars) items within a picture list for each monkey in the serial probe recognition task. The decoding accuracy of the HC and the cERC was higher for initial items than for middle items, whereas the accuracy of the PRC was higher for middle items than for initial items. *$p < 0.05$, **$p < 0.01$. Dashed line: significant prediction accuracy with $p = 0.01$ (binominal-test, population analysis), ○: monkey A, ×: monkey V.

(B) Prediction maps showing the accuracy of the classifications during the serial probe recognition task for each monkey. Regions enclosed in green show significantly high predictability in the single-probe recognition task.

Neural correlates of subsequent memory effects in the monkey MTL identified by univariate analysis

We next examined whether the results of the multi-voxel pattern analysis were consistent with those of conventional univariate analysis. To identify the regions that predicted subsequent recognition performance we compared activity levels during cue periods in which monkeys remembered (later Hit) the item presented during the choice period to activity levels during cue periods in which monkeys forgot (later Miss) the item presented during the choice period in the single-probe recognition task (Figure 12A; later Hit vs. later Miss). In the MTL, bilateral significant peaks were detected in the PRC ($p < 0.05$, FDR corrected within the MTL) and the cERC ($p < 0.05$; Table 4). The activation patterns around the peak in the PRC and cERC detected by the univariate analysis (Figure 12A) also adequately predicted subsequent memory performance by the multivariate decoding analysis (PRC, monkey A: 70%, monkey V: 66%, $p < 0.01$ for both; cERC, monkey A: 66%, monkey V: 63%, $p < 0.05$ for both; Figure 12B). However, the univariate analysis was not sufficiently sensitive to identify the bilateral hippocampi as loci that predicted subsequent memory performance.

Functional dissociation between PRC and cERC during memory encoding ascertained by univariate analysis

Finally, we examined whether the functional dissociation between the PRC and cERC in the serial probe recognition task, whereby the prediction of subsequent memory performance was differentially affected by the position of the cue item in the list, was also detected by univariate analysis (Figure 12C). A subsequent memory effect on the brain activity was significantly observed in the cERC during the encoding of initial items ($p = 0.03$, family-wise error rate

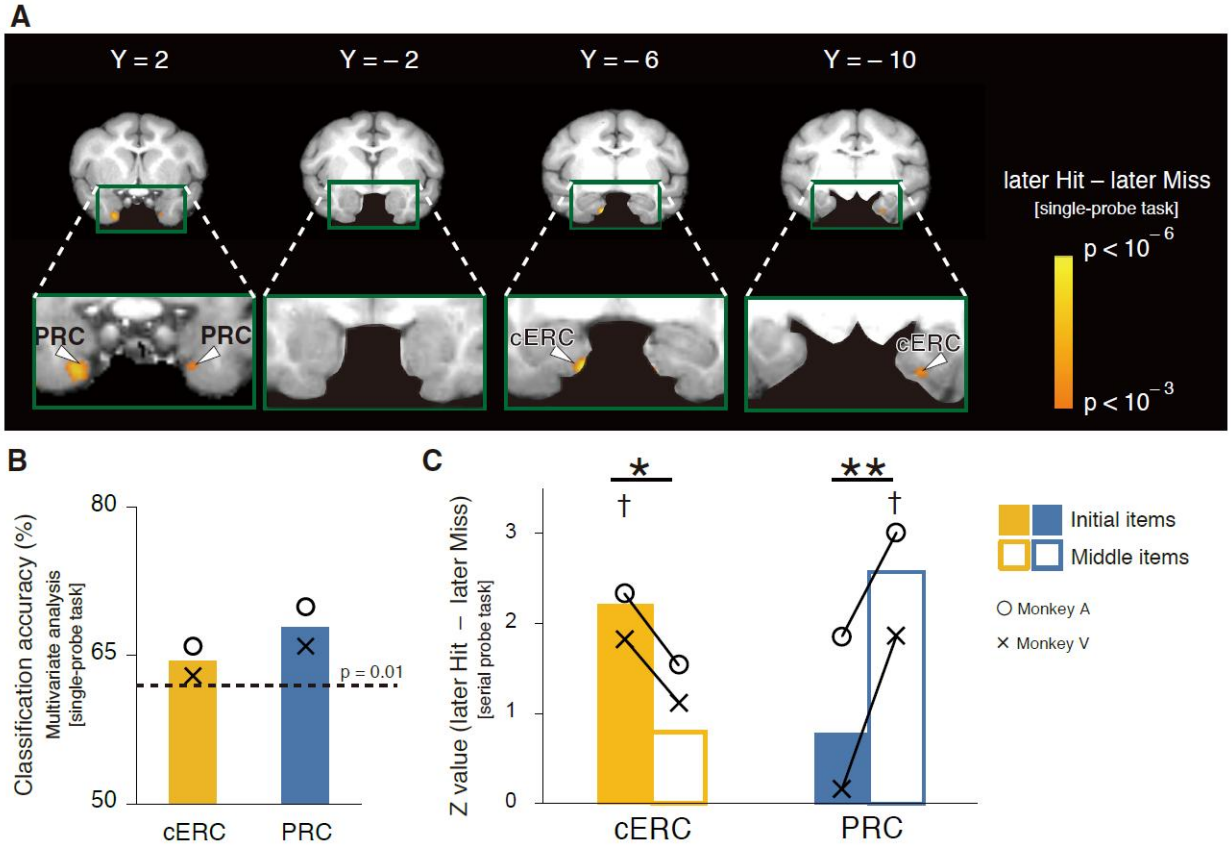

Figure 12. Differential subsequent memory effects between macaque MTL regions identified by univariate analysis.

(A) Activation maps (later Hit > later Miss) for the single-probe recognition task superimposed on coronal sections ($t > 3.1$, $p < 0.001$). PRC: perirhinal cortex, cERC: caudal entorhinal cortex.

(B) Classification accuracy in the activated regions in a 2-mm radius sphere around the peak detected by univariate analysis in the single-probe recognition task (Table 3). Dashed line: significant prediction accuracy with $p = 0.01$ (binominal-test, population analysis), ○: monkey A, ×: monkey V.

(C) Activation values for the "later Hit" trials compared with those in the "later Miss" trials for initial items and middle items in the serial probe recognition task in the cERC (yellow) and the PRC (blue). The activation value of the cERC was higher for initial items than for middle items, whereas the value of the PRC was higher for middle items than for initial items. *$p < 0.05$, **$p < 0.01$. †$p < 0.05$ (FWE corrected, SVC around the activation peaks). ○: monkey A, ×: monkey V.

Table 4 Brain regions activated in "later Hit" > "later Miss" contrasts in the medial temporal lobe during the single-probe recognition task

	X	y	z	T	Area
L	-8	2	-17	4.1	PRC
R	10	2	-16	3.4	
L	-4	-6	-15	4.8	cERC
R	11	-10	-15	3.6	

L = left; R = right; Univariate analysis. Significant peaks with a voxel level of $p < 0.05$ (corrected by false discovery rate) within the medial temporal lobe.

[FWE] corrected, small volume correction [SVC]), but not during the encoding of middle items ($p = 0.35$). Significant subsequent memory-related activity was observed in the PRC during the encoding of middle items ($p = 0.03$), but not during the encoding of initial items ($p > 0.5$). Two-way ANOVA (two positions [initial, middle] × two areas [cERC, PRC]) identified a significant interaction between position and area ($F[2,2] = 4.06\times10^4$, $p = 0.003$), although neither position ($F[1,1] = 7.17$, $p = 0.22$) nor area ($F[1,2] = 0.02$, $p > 0.5$) showed a significant main effect. The cERC and PRC were then dissociated to determine their contribution to encoding items in different positions in the cue list. Tests for simple main effects revealed that the activation value of the cERC ($F[1,2] = 39.0$, $p = 0.02$) was significantly higher for initial items than for middle items, whereas the accuracy of the PRC was significantly higher for middle items than for initial items ($F[1,2] = 134$, $p = 0.007$). These results reproduced the observations from the multivariate decoding analysis (Figure 11A).

To ensure that this functional differentiation between PRC and cERC could not be simply explained by a gross difference in memory recognition accuracy (Figure 1B), or memory strength, we also estimated the correlation between the behavioral performance on each day and brain activity in the two regions (the initial and middle items were analyzed separately) (Figure 13). The fMRI signal in the cERC showed a significant positive correlation with the memory recognition accuracy across the sessions for the initial items ($r = 0.45$, $p = 0.02$), but not for the middle items ($r = -0.08$, $p > 0.5$). In contrast, the fMRI signal in the PRC showed a significant positive correlation with the memory recognition accuracy across sessions for the middle items ($r = 0.39$, $p = 0.04$), but not for the initial items ($r = -0.01$, $p > 0.5$). In summary, the activity of the cERC or PRC was predicted by memory recognition accuracy only when monkeys encoded the initial or middle items, respectively. These results corroborate the existence of two qualitatively

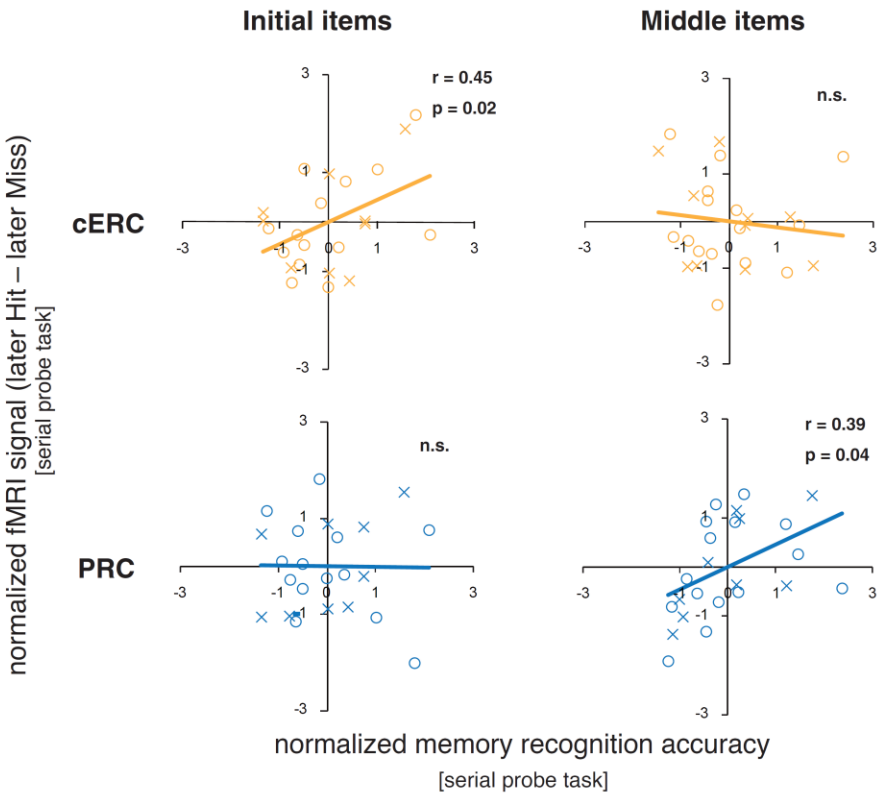

Figure 13. Inter-session correlation between memory accuracy and subsequent memory effect.

Inter-session brain activity in the cERC for initial item retrieval and in the PRC for middle item retrieval was positively correlated with performance. The x-axis shows the memory recognition accuracy (z-transformed) and the y-axis shows the encoding success activity (z-transformed). ○: monkey A, ×: monkey V.

distinct encoding processes in the MTL (Figure 14).

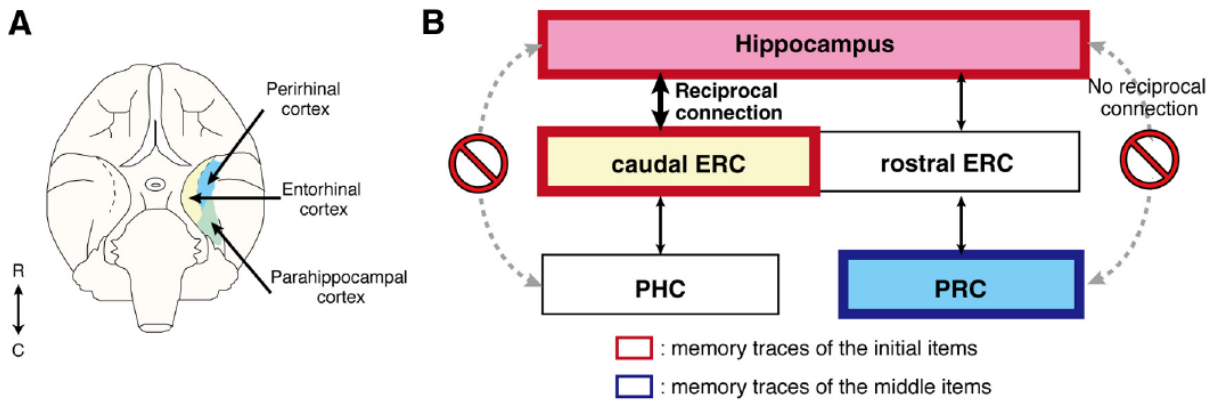

Figure 14. New insights into the primate memory-encoding system obtained from the present study.

(A) The distribution of regions within the medial temporal lobe (blue: perirhinal cortex, yellow: entorhinal cortex, green: parahippocampal cortex) in monkey brain. Modified from Mayford et al. [98]. R: rostral, C: caudal.

(B) Schemata of the primate memory-encoding processes proposed according to results of the present monkey fMRI study. This view of the primate memory-encoding system suggests that memory traces related to initial items are formed in the hippocampus and the caudal ERC, whereas memory traces related to middle items are formed in the PRC. This is consistent with the literature on anatomy of monkeys, which has reported that the hippocampus have major reciprocal direct connections with the caudal ERC but not with the PRC. ERC: entorhinal cortex, PHC: parahippocampal cortex, PRC: perirhinal cortex

Discussion

This study is the first demonstration of awake monkey fMRI experiments during retrieval and encoding of recognition memory. In the former part of the present study, I first identified retrieval-related regions that were active for correct recognition of seen items compared to correct rejection of unseen items (old/new effect). I then found functional dissociation of the monkey retrieval-related regions in PPC, PG/PGOp in IPL and PEa/DIP in IPS, based on the serial position effect. Finally, network analyses for the functional connectivity of task-evoked and spontaneous BOLD activity confirmed that PEa/DIP and PG/PGOp were separately embedded in different brain-wide sub-networks of the retrieval-related regions, and these two sub-networks were also differently characterized by the serial position effect. In the latter part, I first identified encoding success regions that showed a subsequent memory effect in the hippocampus, PRC and cERC by using multi-voxel pattern analysis and conventional univariate analysis. Moreover, these areas were functionally differentiated and responsible for encoding items in different positions.

Hippocampal activity during retrieval and encoding in a serial probe recognition task

In the serial probe recognition task, a typical U-shaped serial position curve of corrected recognition rate accompanied by primacy and recency effects was observed in both monkeys (Figure 1). Human studies have attributed the primacy effect to facility in retrieving the first item that is consolidated in long-term memory during the encoding process [70]. A recent behavioral study suggested that long-term memory processes also elicited the primacy effect in monkeys [44]. Both the retrieval- and encoding-related activity reflecting the primacy effect in the present study (Figures 5, 9, 11, 12) would contribute to long-term episodic memory retrieval in monkeys. Indeed, bilateral hippocampi reflected the primacy effect both during retrieval and encoding.

This modulation of hippocampal activity is consistent with the previous report in humans that specific impairment of the primacy effect but no impairment of recency effect are followed by damage to bilateral hippocampi [45]. Thus, hippocampal activity identified in this study is suggested to be related to long-term memory retrieval.

Furthermore, electrophysiological recordings in the macaque monkeys have shown that the hippocampus plays a role in the encoding of contextual information [71, 72] including spatial location [73] and temporal order [74]. Lesion studies in rats also support these recollection-like roles of the hippocampus [75, 76]. The encoding- and retrieval-related regions that were localized within the hippocampus in this monkey fMRI experiment may reflect contextual processing that effectively works during encoding of the initial item, which is the most distinctive item in a list.

Functional differentiation of memory retrieval-related regions in the parietal and frontal cortices

For retrieval-related network in the parietal cortex, we found retrieval-related activity in the posterior IPL (PG/PGOp) and the IPS (PEa/DIP) (Figure 3, Table 2). These macaque parietal areas have long been considered multimodal processing areas where information from somatosensory and visual cortices is integrated [77, 78]. In the present study, contribution of macaque PPC to recognition memory retrieval was revealed for the first time. In addition, the retrieval-related activities in PG/PGOp and PEa/DIP were dissociated with respect to both response profiles for retrieved cue item positions and effective connectivity with the hippocampus. Anatomically, PG/PGOp is known to receive disynaptic input from the CA1 region of the hippocampus via the parahippocampal gyrus [79]. By contrast, PEa/DIP is known

to receive input from adjacent areas including PO, the ventral lateral intraparietal area (POaI), and dorsal area 5 (PEC) [39], while anatomical connections with hippocampus or parahippocampal gyrus have not been determined. This closer anatomical relationship of hippocampus with PG/PGOp than with PEa/DIP might mediate the enhancement of effective connectivity for the requirement of long-term memory retrieval. In humans, the angular gyrus (Brodmann area 39) in the posterior IPL, which shows the "old/new effect" in memory retrieval, is known to functionally connect with hippocampus [80], and in addition, both angular gyrus and hippocampus demonstrated increased activity during successful episodic retrieval of long-term memory [12, 81]. The identified retrieval-related area in macaque PG/PGOp, which was more highly activated and more strongly connected with hippocampus when retrieval from long-term memory was required, is thus implied to functionally correspond to the human angular gyrus in memory retrieval.

While primacy-effect related activities during retrieval were identified in IPL (PG/PGOp), recency-effect related activities were identified in IPS (PEa/DIP). Electrophysiological studies of macaque DIP neurons [82] reported neuronal activity involved in memorizing sequences of events (numbers), which was further investigated in theoretical studies [83]. These sequence-selective activities of IPS neurons might partially account for the fMRI activity profile of PEa/DIP in the present study, but do not explain our observation that PEa/DIP activity was selective only to the last item retrieval (Figure 5C). Further examinations of the fMRI activity spots in cellular level will clarify the neuronal basis of the differentiation between IPS and IPL regarding the retrieval of items in a sequence.

In the frontal cortex, we identified retrieval-related activity in bilateral dorsolateral (area 9/46V) and ventrolateral (area 44, area 45) prefrontal areas (Figure 3, Table 2). In previous

human studies, specific areas within dorso- and ventrolateral prefrontal cortices are active for the correct recognition of seen items, and are suggested to play differential roles in the selection of memory representation and post-retrieval monitoring during both episodic and working memory processes (for reviews see [84, 85]). The tendency of these frontal regions to be active for retrieval of the last items in this study (Figure 9C) reflects their responsibility for the retrieval of recently encoded items, which might be actively maintained in the working memory. In addition, these prefrontal areas were functionally dissociated from area 8B which is participated in the default-mode network in monkeys, as with in humans. It will be of great interest to study how these frontal areas work cooperatively with PEa/DIP during retrieval from working memory.

Correspondence of function- and sub-network-level differentiation in the memory retrieval network

Recently, the role of the PPC has been associated with top-down and bottom-up attention during memory processes in humans [10, 86, 87]. Ventral PPC is thought to be involved in reorienting attention to memory via "bottom-up" pathways, while dorsal PPC is thought to be involved in reorienting attention to memory via "top-down" pathways in humans. In the present study, the PPI analyses (Figures 5F, 6) showed contrasting results between the two macaque PPC areas, which suggest bottom-up attention from the hippocampus to the IPL (Figure 5F), and top-down attention from the IPS to V4 (Figure 6). These results were consistent with this model of human PPC functions.

Analysis of spontaneous BOLD activity revealed that functional dissociation within the macaque PPC was accompanied by network-level dissociation (Figures 7D, 9B, 9C). Human studies have shown that each of functional networks identified from spontaneous BOLD activity

matches a set of brain regions that cooperate during active cognitive tasks [88]. In the present monkey study, the two retrieval-related areas in PPC, PG/PGOp and PEa/DIP, were embedded in distinct sub-groups: the former was functionally connected with the superior branch of arcuate sulcus (area 8B), posterior cingulate cortex (area 23, PECg), and temporoparietal areas (Tpt) (module 2, pink, Figure 7D), while the latter was mainly connected with the lateral prefrontal cortex (area 45B, 9/46V) (module 3, light blue, Figure 7D). The areas included in module 2 (area 23, PECg [PEci], IPa, and Tpt) exhibited anatomical connection with PG (PG-injection cases, 20, 27, and 29 in Rozzi et al. [89]). The dependency of the retrieval-related activity on retrieved item position differed between these modules: module 2 including PG/PGOp reflected the primacy effect, while module 3 including PEa/DIP reflected the recency effect. Module 2 was included in the functional connectivity map for the seed of posterior cingulate/precuneus cortex, which is known as the "default-mode network" of monkeys [21, 90]. Area 8B and area 23 in module 2 are especially known to reduce its activity during performance of goal-directed tasks [90]. In humans, the default-mode network is associated with episodic memory function [80]. The angular gyrus, which is activated during episodic memory retrieval, is included in the network, and is suggested to act as one of the hubs [46]. Their participation in the default-mode network will provide additional evidence for the functional correspondence between the macaque PG/PGOp and human angular gyrus. Meanwhile, module 3 was included in the fronto-parietal network (for humans, see [87]; for monkeys, see [91]). In humans, this network is considered to be related to top-down attention [87]. The human intraparietal regions, which are activated during working memory retrieval and mediate memory control processes, are included in the network [10, 46]. This inter-species correspondence in terms of the cognitive role and functional connectivity with the frontal cortex suggests that the human counterpart of macaque PEa/DIP resides in the human

intraparietal regions. Further work will establish the functional correspondence between retrieval-related PPC in humans and macaques.

Functional differentiation of memory encoding-related regions in MTL

We localized an encoding success region within the cERC in monkeys. As it is for the hippocampus, the cERC was responsible for encoding the initial item in the list, which is related to the primacy effect. The cERC is known to strongly project to the hippocampus, and to receive major cortical input from parahippocampal and retrosplenial cortices rather than from the PRC [68]. The observation that the cERC, along with the hippocampus, was functionally differentiated from the PRC during memory encoding is consistent with the literature on brain anatomy of macaque monkeys [68].

Unlike the hippocampus, involvement of the cERC in memory encoding has rarely been reported in humans, likely because the precise demarcation of the entorhinal cortex located on the human parahippocampal gyrus from other cortices is difficult due to the scarcity of MRI-based boundary delineations in the gyrus (for anatomy and nomenclatures of these regions, see **Materials and Methods** in **Part II**). Recent human fMRI studies have shown that the middle parahippocampal gyrus is responsible for contextual or scene processing, whereas the anterior parahippocampal gyrus is not [92, 93]. The present monkey study suggests a possibility that the middle part of parahippocampal gyrus in humans, which is repeatedly referred to as the ‘parahippocampal cortex’, corresponds to the macaque caudal entorhinal cortex. In monkeys, the entorhinal cortex distributes at a higher level than the parahippocampal cortex in the hierarchical processing network that is shaped by anatomical connectivity patterns [94]. Therefore, the process of encoding recollection-based memory may occur in an area anatomically closer to the

hippocampus and hierarchically higher than previously believed (Figure 14). This would redefine the memory encoding network in the primate MTL.

We also localized an encoding success region within area 36 of the PRC. The PRC was responsible for encoding items presented in the middle of the cue list. For these middle items the monkeys may have adopted encoding strategies based on familiarity rather than recollection because they were less likely to utilize distinctiveness within a picture list, or contextual information, to encode middle items than they were to encode initial items. Electrophysiological studies in monkeys have shown that area 36 contains neurons that represent visual long-term memory [95] and that the activity of these neurons was different for familiar and new stimuli [96, 97]. The encoding success regions localized within the PRC in this monkey fMRI study may reflect neuronal correlates such as these.

Future directions

In the present study, the brain regions involved in primacy and recency effects were represented not only in the level of specific brain regions but also in the level of modules, each of which consists of functionally connected areas. This network-level dissociation suggested that the primacy and recency effects reflected two distinct memory processes [13, 45] and would not be explained by a single mechanism based on relative temporal distinctiveness or on context variability. However, serial position effect is complex and actually influenced by various cognitive processes depending on task conditions. In humans, differential activity profiles of dorsal and ventral PPC were shown as a function of retrieval delay [12], but the profiles were varied depending on task [13]. Therefore, to establish the monkey counterparts of the human retrieval success areas that were typically identified in long-term memory paradigms, it is needed

to examine further primacy effect-related activity in other task conditions which require long-term memory processes

In this study, we combined fMRI activation analysis and connectivity analyses based on task-evoked and spontaneous BOLD activities. All these analyses converged to reveal the functional dissociation within PPC during memory retrieval in monkeys. The multimodal approach in combination with connectivity-based methods is useful to characterize and classify brain regions cooperatively interacting for specific functions. Furthermore, network-level analysis in monkeys whose anatomical structure is well known will provide important clues to understanding the relationship between functionally identified networks and structural anatomical networks at a level unattainable with experimentation in humans.

I also precisely localized and characterized the MTL sites responsible for memory encoding in monkeys on the basis of literatures on anatomy. These findings, providing precise localization of memory traces in monkeys, bridge the gap between imaging studies on humans and anatomical studies on non-human primates and can accelerate fine electrophysiological characterization of memory traces in the monkey MTL.

Acknowledgments

This thesis project is achieved from collaboration with Dr. Takahiro Osada, Dr. Yusuke Adachi, Dr. Teppei Matsui, Dr. Takamitsu Watanabe, Dr. Hiroko, M. Kimura, Dr. Rieko Setuie, and Prof. Yasushi Miyashita. I greatly appreciate the collaborators. One Japanese monkey used in this research was provided by NBRP "Japanese Monkeys" through the National BioResource Project of the MEXT. I thank Tomomi Watanabe for technical assistance and Dr. Seiki Konishi for helpful comments on the manuscript. A part of this thesis was published as an article in *Neuron* (10.1016/j.neuron.2012.12.019) and as an article in *The Journal of Neuroscience* (10.1523/JNEUROSCI.4048-13.2014).

References

1. Kagan, I., Iyer, A., Lindner, A., and Andersen, R.A. (2010). Space representation for eye movements is more contralateral in monkeys than in humans. Proc. Natl. Acad. Sci. U. S. A. *107*, 7933-7938.
2. Koyama, M., Hasegawa, I., Osada, T., Adachi, Y., Nakahara, K., and Miyashita, Y. (2004). Functional magnetic resonance imaging of macaque monkeys performing visually guided saccade tasks: comparison of cortical eye fields with humans. Neuron *41*, 795-807.
3. Logothetis, N.K., Guggenberger, H., Peled, S., and Pauls, J. (1999). Functional imaging of the monkey brain. Nat. Neurosci. *2*, 555-562.
4. Nakahara, K., Hayashi, T., Konishi, S., and Miyashita, Y. (2002). Functional MRI of macaque monkeys performing a cognitive set-shifting task. Science *295*, 1532-1536.
5. Pinsk, M.A., DeSimone, K., Moore, T., Gross, C.G., and Kastner, S. (2005). Representations of faces and body parts in macaque temporal cortex: a functional MRI study. Proc. Natl. Acad. Sci. U. S. A. *102*, 6996-7001.
6. Tsao, D.Y., Freiwald, W.A., Knutsen, T.A., Mandeville, J.B., and Tootell, R.B.H. (2003). Faces and objects in macaque cerebral cortex. Nat. Neurosci. *6*, 989-995.
7. Curtis, C.E., and D'Esposito, M. (2003). Persistent activity in the prefrontal cortex during working memory. Trends. Cogn. Sci. *7*, 415-423.
8. Squire, L.R., Stark, C.E.L., and Clark, R.E. (2004). The medial temporal lobe. Annu. Rev. Neurosci. *27*, 279-306.
9. Konishi, S., Wheeler, M.E., Donaldson, D.I., and Buckner, R.L. (2000). Neural correlates of episodic retrieval success. NeuroImage *12*, 276-286.
10. Vilberg, K.L., and Rugg, M.D. (2008). Memory retrieval and the parietal cortex: a review

of evidence from a dual-process perspective. Neuropsychologia *46*, 1787-1799.

11. Wright, A.A., Santiago, H.C., Sands, S.F., Kendrick, D.F., and Cook, R.G. (1985). Memory processing of serial lists by pigeons, monkeys, and people. Science *229*, 287-289.

12. Huijbers, W., Pennartz, C.M.A., and Daselaar, S.M. (2010). Dissociating the "retrieval success" regions of the brain: effects of retrieval delay. Neuropsychologia *48*, 491-497.

13. Talmi, D., Grady, C.L., Goshen-Gottstein, Y., and Moscovitch, M. (2005). Neuroimaging the serial position curve. A test of single-store versus dual-store models. Psychol. Sci. *16*, 716-723.

14. Isoda, M., Tsutsui, K.-I., Katsuyama, N., Naganuma, T., Saito, N., Furusawa, Y., Mushiake, H., Taira, M., and Tanji, J. (2005). Design of a head fixation device for experiments in behaving monkeys. J. Neurosci. Methods. *141*, 277-282.

15. Koyano, K.W., Machino, A., Takeda, M., Matsui, T., Fujimichi, R., Ohashi, Y., and Miyashita, Y. (2011). In vivo visualization of single-unit recording sites using MRI-detectable elgiloy deposit marking. J. Neurophysiol. *105*, 1380-1392.

16. Matsui, T., Tamura, K., Koyano, K.W., Takeuchi, D., Adachi, Y., Osada, T., and Miyashita, Y. (2011). Direct comparison of spontaneous functional connectivity and effective connectivity measured by intracortical microstimulation: an fMRI study in macaque monkeys. Cereb. Cortex *21*, 2348-2356.

17. Kamigaki, T., Fukushima, T., and Miyashita, Y. (2009). Cognitive set reconfiguration signaled by macaque posterior parietal neurons. Neuron *61*, 941-951.

18. Adachi, Y., Osada, T., Sporns, O., Watanabe, T., Matsui, T., Miyamoto, K., and Miyashita, Y. (2011). Functional connectivity between anatomically unconnected areas is shaped by

collective network-level effects in the macaque cortex. Cereb. Cortex.

19. Matsui, T., Koyano, K.W., Koyama, M., Nakahara, K., Takeda, M., Ohashi, Y., Naya, Y., and Miyashita, Y. (2007). MRI-based localization of electrophysiological recording sites within the cerebral cortex at single-voxel accuracy. Nat. Methods. *4*, 161-168.

20. Matsui, T., Koyano, K.W., Tamura, K., Osada, T., Adachi, Y., Miyamoto, K., Chikazoe, J., Kamigaki, T., and Miyashita, Y. (2012). FMRI activity in the macaque cerebellum evoked by intracortical microstimulation of the primary somatosensory cortex: evidence for polysynaptic propagation. PLoS One *7*, e47515.

21. Vincent, J.L., Patel, G.H., Fox, M.D., Snyder, A.Z., Baker, J.T., Van Essen, D.C., Zempel, J.M., Snyder, L.H., Corbetta, M., and Raichle, M.E. (2007). Intrinsic functional architecture in the anaesthetized monkey brain. Nature *447*, 83-86.

22. Donaldson, D.I., Wheeler, M.E., and Petersen, S.E. (2010). Remember the source: dissociating frontal and parietal contributions to episodic memory. J. Cogn. Neurosci. *22*, 377-391.

23. Genovese, C.R., Lazar, N.A., and Nichols, T. (2002). Thresholding of statistical maps in functional neuroimaging using the false discovery rate. NeuroImage *15*, 870-878.

24. Paxinos, G., Huang, X.F., Petrides, M., and Toga, A.W. (2008). The rhesus monkey brain in stereotactic coordinates, (London, UK: Elsevier Academic).

25. Friston, K.J., Penny, W.D., and Glaser, D.E. (2005). Conjunction revisited. NeuroImage *25*, 661-667.

26. Nichols, T., Brett, M., Andersson, J., Wager, T., and Poline, J.B. (2005). Valid conjunction inference with the minimum statistic. NeuroImage *25*, 653-660.

27. Nelissen, K., and Vanduffel, W. (2011). Grasping-related functional magnetic resonance

imaging brain responses in the macaque monkey. J Neurosci *31*, 8220-8229.

28. Peeters, R., Simone, L., Nelissen, K., Fabbri-Destro, M., Vanduffel, W., Rizzolatti, G., and Orban, G.A. (2009). The representation of tool use in humans and monkeys: common and uniquely human features. J Neurosci *29*, 11523-11539.

29. Gregoriou, G.G., Borra, E., Matelli, M., and Luppino, G. (2006). Architectonic organization of the inferior parietal convexity of the macaque monkey. J Comp Neurol *496*, 422-451.

30. Friston, K.J., Buechel, C., Fink, G.R., Morris, J., Rolls, E., and Dolan, R.J. (1997). Psychophysiological and modulatory interactions in neuroimaging. NeuroImage *6*, 218-229.

31. Wardak, C., Vanduffel, W., and Orban, G.A. (2010). Searching for a salient target involves frontal regions. Cereb Cortex *20*, 2464-2477.

32. Ninomiya, T., Sawamura, H., Inoue, K., and Takada, M. (2012). Segregated pathways carrying frontally derived top-down signals to visual areas MT and V4 in macaques. J Neurosci *32*, 6851-6858.

33. Buckner, R.L., Andrews-Hanna, J.R., and Schacter, D.L. (2008). The brain's default network: anatomy, function, and relevance to disease. Ann. N. Y. Acad. Sci. *1124*, 1-38.

34. Fox, M.D., Snyder, A.Z., Vincent, J.L., Corbetta, M., Van Essen, D.C., and Raichle, M.E. (2005). The human brain is intrinsically organized into dynamic, anticorrelated functional networks. Proc. Natl. Acad. Sci. U. S. A. *102*, 9673-9678.

35. Fair, D.A., Schlaggar, B.L., Cohen, A.L., Miezin, F.M., Dosenbach, N.U., Wenger, K.K., Fox, M.D., Snyder, A.Z., Raichle, M.E., and Petersen, S.E. (2007). A method for using blocked and event-related fMRI data to study "resting state" functional connectivity.

NeuroImage *35*, 396-405.

36. Kimura, H.M., Hirose, S., Kunimatsu, A., Chikazoe, J., Jimura, K., Watanabe, T., Abe, O., Ohtomo, K., Miyashita, Y., and Konishi, S. (2010). Differential temporo-parietal cortical networks that support relational and item-based recency judgments. NeuroImage *49*, 3474-3480.

37. McKeown, M.J., Hansen, L.K., and Sejnowsk, T.J. (2003). Independent component analysis of functional MRI: what is signal and what is noise? Curr Opin Neurobiol *13*, 620-629.

38. McKeown, M.J., and Sejnowski, T.J. (1998). Independent component analysis of fMRI data: examining the assumptions. Hum Brain Mapp *6*, 368-372.

39. Lewis, J.W., and Van Essen, D.C. (2000). Corticocortical connections of visual, sensorimotor, and multimodal processing areas in the parietal lobe of the macaque monkey. J. Comp. Neurol. *428*, 112-137.

40. Stephan, K.E., Kamper, L., Bozkurt, A., Burns, G.A., Young, M.P., and Kotter, R. (2001). Advanced database methodology for the Collation of Connectivity data on the Macaque brain (CoCoMac). Philos Trans R Soc Lond B Biol Sci *356*, 1159-1186.

41. Newman, M.E.J. (2006). Finding community structure in networks using the eigenvectors of matrices. Phys. Rev. E. Stat. Nonlin. Soft. Matter. Phys. *74*, 036104.

42. Rubinov, M., and Sporns, O. (2011). Weight-conserving characterization of complex functional brain networks. NeuroImage *56*, 2068-2079.

43. Rubinov, M., and Sporns, O. (2010). Complex network measures of brain connectivity: uses and interpretations. NeuroImage *52*, 1059-1069.

44. Basile, B.M., and Hampton, R.R. (2010). Rhesus monkeys (Macaca mulatta) show robust

primacy and recency in memory for lists from small, but not large, image sets. Behav. Processes *83*, 183-190.

45. Baddeley, A.D., and Warrington, E.K. (1970). Amnesia and the distinction between long- and short-term memory. J. Verb. Learn. Verb. Behav. *9*, 176-189.

46. Nelson, S.M., Cohen, A.L., Power, J.D., Wig, G.S., Miezin, F.M., Wheeler, M.E., Velanova, K., Donaldson, D.I., Phillips, J.S., and Schlaggar, B.L. (2010). A parcellation scheme for human left lateral parietal cortex. Neuron *67*, 156-170.

47. Hassabis, D., Chu, C., Rees, G., Weiskopf, N., Molyneux, P.D., and Maguire, E.A. (2009). Decoding neuronal ensembles in the human hippocampus. Curr Biol *19*, 546-554.

48. Haynes, J.D., and Rees, G. (2005). Predicting the orientation of invisible stimuli from activity in human primary visual cortex. Nat Neurosci *8*, 686-691.

49. Johnson, J.D., McDuff, S.G., Rugg, M.D., and Norman, K.A. (2009). Recollection, familiarity, and cortical reinstatement: a multivoxel pattern analysis. Neuron *63*, 697-708.

50. Kamitani, Y., and Tong, F. (2005). Decoding the visual and subjective contents of the human brain. Nat Neurosci *8*, 679-685.

51. Kay, K.N., Naselaris, T., Prenger, R.J., and Gallant, J.L. (2008). Identifying natural images from human brain activity. Nature *452*, 352-355.

52. Mitchell, T.M., Shinkareva, S.V., Carlson, A., Chang, K.M., Malave, V.L., Mason, R.A., and Just, M.A. (2008). Predicting human brain activity associated with the meanings of nouns. Science *320*, 1191-1195.

53. Watanabe, T., Hirose, S., Wada, H., Katsura, M., Chikazoe, J., Jimura, K., Imai, Y., Machida, T., Shirouzu, I., Miyashita, Y., et al. (2011). Prediction of subsequent recognition performance using brain activity in the medial temporal lobe. Neuroimage *54*,

3085-3092.

54. Wagner, A.D., Schacter, D.L., Rotte, M., Koutstaal, W., Maril, A., Dale, A.M., Rosen, B.R., and Buckner, R.L. (1998). Building memories: remembering and forgetting of verbal experiences as predicted by brain activity. Science *281*, 1188-1191.

55. Burwell, R.D. (2000). The parahippocampal region: corticocortical connectivity. Ann N Y Acad Sci *911*, 25-42.

56. Van Hoesen, G.W., Augustinack, J.C., Dierking, J., Redman, S.J., and Thangavel, R. (2000). The parahippocampal gyrus in Alzheimer's disease. Clinical and preclinical neuroanatomical correlates. Ann N Y Acad Sci *911*, 254-274.

57. Suzuki, W.A., and Amaral, D.G. (1994). Perirhinal and parahippocampal cortices of the macaque monkey: cortical afferents. J Comp Neurol *350*, 497-533.

58. Suzuki, W.A., and Amaral, D.G. (2003). Where are the perirhinal and parahippocampal cortices? A historical overview of the nomenclature and boundaries applied to the primate medial temporal lobe. Neuroscience *120*, 893-906.

59. Suzuki, W.A., and Amaral, D.G. (2003). Perirhinal and parahippocampal cortices of the macaque monkey: cytoarchitectonic and chemoarchitectonic organization. J Comp Neurol *463*, 67-91.

60. Suzuki, W.A., and Amaral, D.G. (1994). Topographic organization of the reciprocal connections between the monkey entorhinal cortex and the perirhinal and parahippocampal cortices. J Neurosci *14*, 1856-1877.

61. Ding, S.L., and Van Hoesen, G.W. (2010). Borders, extent, and topography of human perirhinal cortex as revealed using multiple modern neuroanatomical and pathological markers. Hum Brain Mapp *31*, 1359-1379.

62. Augustinack, J.C., Huber, K.E., Stevens, A.A., Roy, M., Frosch, M.P., van der Kouwe, A.J., Wald, L.L., Van Leemput, K., McKee, A.C., and Fischl, B. (2013). Predicting the location of human perirhinal cortex, Brodmann's area 35, from MRI. Neuroimage *64*, 32-42.

63. Meunier, M., Hadfield, W., Bachevalier, J., and Murray, E.A. (1996). Effects of rhinal cortex lesions combined with hippocampectomy on visual recognition memory in rhesus monkeys. J Neurophysiol *75*, 1190-1205.

64. Murray, E.A., and Mishkin, M. (1986). Visual recognition in monkeys following rhinal cortical ablations combined with either amygdalectomy or hippocampectomy. J Neurosci *6*, 1991-2003.

65. Kondo, H., Saleem, K.S., and Price, J.L. (2003). Differential connections of the temporal pole with the orbital and medial prefrontal networks in macaque monkeys. J Comp Neurol *465*, 499-523.

66. Kondo, H., Saleem, K.S., and Price, J.L. (2005). Differential connections of the perirhinal and parahippocampal cortex with the orbital and medial prefrontal networks in macaque monkeys. J Comp Neurol *493*, 479-509.

67. Saleem, K.S., Kondo, H., and Price, J.L. (2008). Complementary circuits connecting the orbital and medial prefrontal networks with the temporal, insular, and opercular cortex in the macaque monkey. J Comp Neurol *506*, 659-693.

68. Amaral, D.G., Insausti, R., and Cowan, W.M. (1987). The entorhinal cortex of the monkey: I. Cytoarchitectonic organization. J Comp Neurol *264*, 326-355.

69. Blatt, G.J., Pandya, D.N., and Rosene, D.L. (2003). Parcellation of cortical afferents to three distinct sectors in the parahippocampal gyrus of the rhesus monkey: an anatomical

and neurophysiological study. J Comp Neurol *466*, 161-179.

70. Atkinson, R.C., and Shiffrin, R.M. (1968). Human memory: a proposed system and its control processes. In Psychology of Learning and Motivation, Volume Volume 2, W.S. Kenneth and S. Janet Taylor, eds. (Academic Press), pp. 89-195.

71. Suzuki, W.A., and Eichenbaum, H. (2000). The neurophysiology of memory. Ann N Y Acad Sci *911*, 175-191.

72. Brown, M.W., and Aggleton, J.P. (2001). Recognition memory: what are the roles of the perirhinal cortex and hippocampus? Nat Rev Neurosci *2*, 51-61.

73. Rolls, E.T. (1999). Spatial view cells and the representation of place in the primate hippocampus. Hippocampus *9*, 467-480.

74. Naya, Y., and Suzuki, W.A. (2011). Integrating what and when across the primate medial temporal lobe. Science *333*, 773-776.

75. Fortin, N.J., Wright, S.P., and Eichenbaum, H. (2004). Recollection-like memory retrieval in rats is dependent on the hippocampus. Nature *431*, 188-191.

76. Crystal, J.D., Alford, W.T., Zhou, W., and Hohmann, A.G. (2013). Source memory in the rat. Curr Biol *23*, 387-391.

77. Andersen, R.A., and Buneo, C.A. (2002). Intentional maps in posterior parietal cortex. Annu. Rev. Neurosci. *25*, 189-220.

78. Bisley, J.W., and Goldberg, M.E. (2010). Attention, intention, and priority in the parietal lobe. Annu. Rev. Neurosci. *33*, 1-21.

79. Clower, D.M., West, R.A., Lynch, J.C., and Strick, P.L. (2001). The inferior parietal lobule is the target of output from the superior colliculus, hippocampus, and cerebellum. J. Neurosci. *21*, 6283-6291.

80. Vincent, J.L., Snyder, A.Z., Fox, M.D., Shannon, B.J., Andrews, J.R., Raichle, M.E., and Buckner, R.L. (2006). Coherent spontaneous activity identifies a hippocampal-parietal memory network. J. Neurophysiol. *96*, 3517-3531.

81. Yonelinas, A.P., Otten, L.J., Shaw, K.N., and Rugg, M.D. (2005). Separating the brain regions involved in recollection and familiarity in recognition memory. J. Neurosci. *25*, 3002-3008.

82. Nieder, A. (2005). Counting on neurons: the neurobiology of numerical competence. Nat Rev Neurosci *6*, 177-190.

83. Botvinick, M., and Watanabe, T. (2007). From numerosity to ordinal rank: a gain-field model of serial order representation in cortical working memory. J Neurosci *27*, 8636-8642.

84. Cabeza, R., and Nyberg, L. (2000). Imaging cognition II: an empirical review of 275 PET and fMRI studies. J. Cogn. Neurosci. *12*, 1-47.

85. Petrides, M. (2005). Lateral prefrontal cortex: architectonic and functional organization. Philos. Trans. R. Soc. Lond. B. Biol. Sci. *360*, 781-795.

86. Cabeza, R., Ciaramelli, E., Olson, I.R., and Moscovitch, M. (2008). The parietal cortex and episodic memory: an attentional account. Nat. Rev. Neurosci. *9*, 613-625.

87. Corbetta, M., and Shulman, G.L. (2002). Control of goal-directed and stimulus-driven attention in the brain. Nat Rev Neurosci *3*, 201-215.

88. Smith, S.M., Fox, P.T., Miller, K.L., Glahn, D.C., Fox, P.M., Mackay, C.E., Filippini, N., Watkins, K.E., Toro, R., Laird, A.R., et al. (2009). Correspondence of the brain's functional architecture during activation and rest. Proc. Natl. Acad. Sci. U. S. A. *106*, 13040-13045.

89. Rozzi, S., Calzavara, R., Belmalih, A., Borra, E., Gregoriou, G.G., Matelli, M., and Luppino, G. (2006). Cortical connections of the inferior parietal cortical convexity of the macaque monkey. Cereb Cortex *16*, 1389-1417.

90. Mantini, D., Gerits, A., Nelissen, K., Durand, J.B., Joly, O., Simone, L., Sawamura, H., Wardak, C., Orban, G.A., Buckner, R.L., et al. (2011). Default mode of brain function in monkeys. J. Neurosci. *31*, 12954-12962.

91. Hutchison, R.M., Leung, L.S., Mirsattari, S.M., Gati, J.S., Menon, R.S., and Everling, S. (2011). Resting-state networks in the macaque at 7T. NeuroImage *56*, 1546-1555.

92. Staresina, B.P., Duncan, K.D., and Davachi, L. (2011). Perirhinal and parahippocampal cortices differentially contribute to later recollection of object- and scene-related event details. J Neurosci *31*, 8739-8747.

93. Hannula, D.E., Libby, L.A., Yonelinas, A.P., and Ranganath, C. (2013). Medial temporal lobe contributions to cued retrieval of items and contexts. Neuropsychologia.

94. Felleman, D.J., and Van Essen, D.C. (1991). Distributed hierarchical processing in the primate cerebral cortex. Cereb Cortex *1*, 1-47.

95. Miyashita, Y. (1988). Neuronal correlate of visual associative long-term memory in the primate temporal cortex. Nature *335*, 817-820.

96. Li, L., Miller, E.K., and Desimone, R. (1993). The representation of stimulus familiarity in anterior inferior temporal cortex. J Neurophysiol *69*, 1918-1929.

97. Xiang, J.Z., and Brown, M.W. (1998). Differential neuronal encoding of novelty, familiarity and recency in regions of the anterior temporal lobe. Neuropharmacology *37*, 657-676.

98. Mayford, M., Mansuy, I.M., Muller, R.U., and Kandel, E.R. (1997). Memory and

behavior: a second generation of genetically modified mice. Curr Biol *7*, R580-589.